

# Transportation Sector: Urban Area-level Road Emissions

Tomek Kott<sup>1,2</sup>, Kevin Foster<sup>1,2</sup>, Elizabeth Reilly<sup>1,2</sup> and  
Marisa Hughes<sup>1,2</sup>

1) The Johns Hopkins University Applied Physics Laboratory (JHU/APL)

2) The Climate TRACE Coalition



## 1. Introduction

Transportation contributed 27% of anthropogenic greenhouse gas (GHG) emissions in the United States of America (USA) for 2020, higher than any other sector, and 12.6% of all global GHG emissions in 2019 (US EPA 2023; World Resources Institute 2022). The primary source of transportation sector emissions are on-road vehicles, accounting for approximately 74% of global transportation emissions in 2018 (International Energy Agency 2019). Quantifying the distribution of on-road transportation emissions and creating timely emissions inventories are vital to identify trends, track mitigation efforts, and inform policy decisions.

Previous efforts have developed detailed bottom-up on-road emission inventories for the USA (Gately, Hutyra, and Wing 2019; Gurney et al. 2020), but do not easily extend globally due to the reliance on vehicle traffic and road data that is not always readily available. The Emissions Database for Global Atmospheric Research (EDGAR) provides a global inventory for transportation that uses road density as a proxy to spatially distribute emissions (Crippa et al. 2020). However, some emission estimates for urban centers in EDGAR deviated from other bottom-up inventories by 500%, indicating that road density is not a sufficient proxy for global high-resolution inventories (Gately, Hutyra, and Wing 2015). Carbon Monitor is a global emissions inventory that utilizes a variety of activity data to estimate daily GHG emissions, however the reliance on proprietary traffic data in the ground transportation sector limits the ability to extend to locations where this data is not available (Liu et al. 2020). Other methods have used machine learning (ML) to directly predict emissions, but their ability to generalize globally is unclear (Mukherjee et al. 2021; Scheibenreif, Mommert, and Borth 2021).

JHU/APL has developed an approach to estimate road transportation emissions, and applied this methodology to 10,000 global urban areas, representing nearly 45% of the world's population. Our "hybrid" algorithm leverages the strengths of ML applied to remote sensing data, in addition to incorporating region-specific emissions factors (EFs) data to create scalable and transparent emissions estimations globally. A detailed description of our method, data sources, and validation results is contained herein.

## 2. Data and Methods

### 2.1. Overview

Our hybrid emissions estimation method was primarily composed of two parts: a set of ML models trained to predict road transport activity, and an emissions factors (EFs) pipeline that converts activity predictions to emissions estimates. This approach combines the strengths of satellite imagery and ML with traditional “bottom-up” emissions inventories that directly incorporate vehicle fleet mix, fuel efficiency, and other EF data. Having these two, primarily independent parts affords continuous improvement of each as newer and better data become available. A high-level system architecture is shown below in Figure 1.

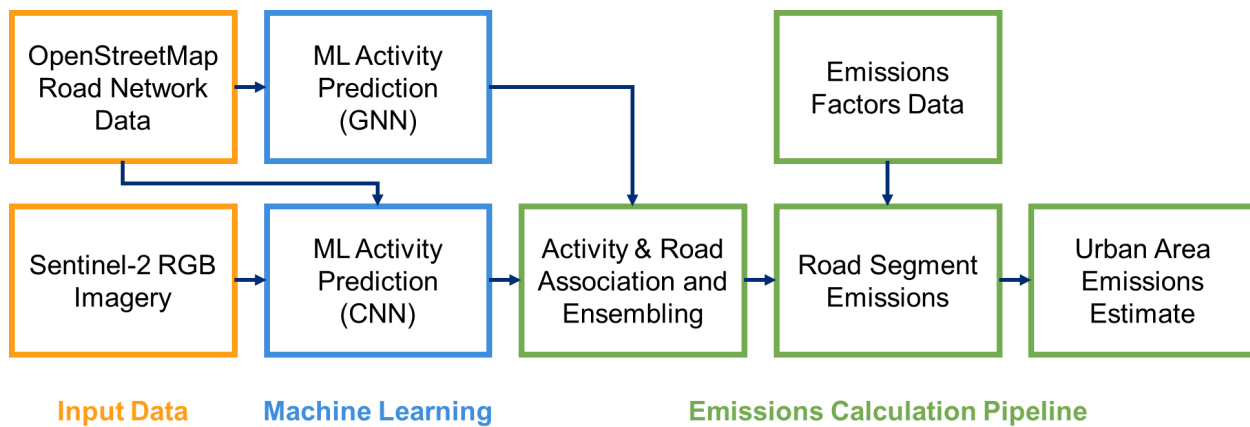


**Figure 1** Emissions estimation architecture overview.

Remote sensing and geospatial data were fed to two different ML models; a convolutional neural network (CNN) based model and a graph neural network (GNN) based model. This provides more complete and higher frequency estimates of average annual daily traffic (AADT). These AADT predictions were then assigned to their corresponding road segment based on the known geographic location of the underlying road network. Values from the two different models were ensembled via averaging. EFs were computed a priori from a curated database of road and vehicle-related data for a specific region, assigning EF values to each type of road in a city; see Sections 2.2.5, 2.2.7, and 2.2.8. Estimated AADT was converted to total vehicle kilometers traveled (VKT) using the known length of each road segment, and then multiplied by the appropriate EF for this road type. This process was repeated and summed over all road segments in a city to calculate the final, total emissions estimate for that urban area for 2021 and 2022. This process is shown below in Figure 2.

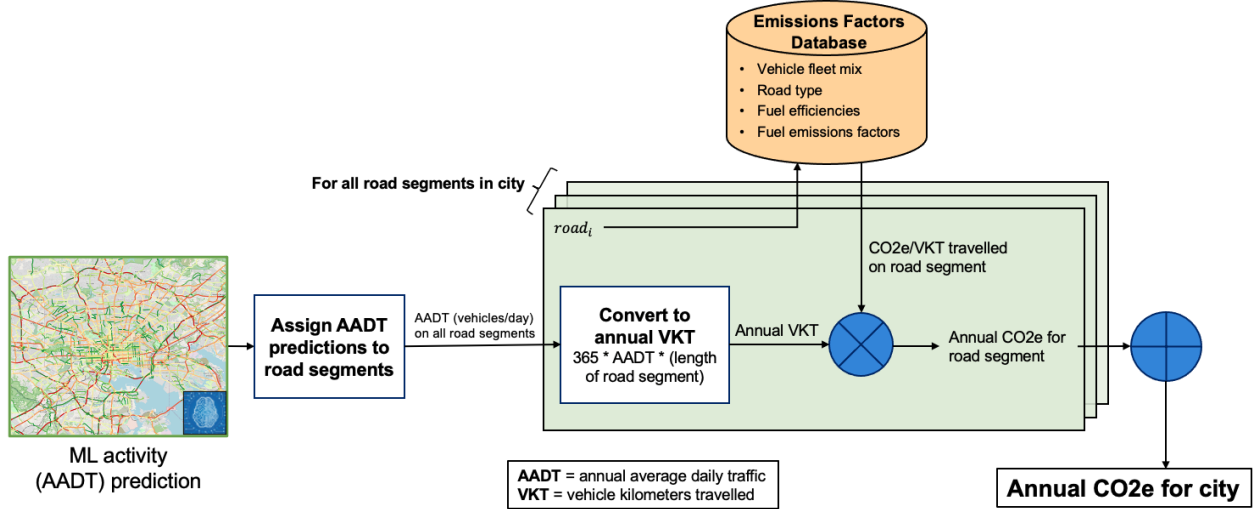


**Figure 2** Converting ML-predicted road traffic to emissions.

## 2.2. Data

### 2.2.1. Urban Center Selection

We utilized the European Union Joint Research Center Global Human Settlement Layer Urban Centers Database (GHSL-UCDB) dataset for a globally consistent representation of urban center extent (Florczyk et al. 2019). This database contains approximately 13,000 urban centers worldwide, and utilizes a definition of urban center based on population density and built up area. Specifically, an urban center was defined as “the spatially-generalized high-density clusters of contiguous grid cells of 1 km<sup>2</sup> with a density of at least 1,500 inhabitants per km<sup>2</sup> of land surface or at least 50% built-up surface share per km<sup>2</sup> of land surface, and a minimum population of 50,000.” (Florczyk et al. 2019). Due to this definition, urban center geometries in UCDB often have significantly different shapes and sizes as compared to official administrative bounds of cities, e.g., from OpenStreetMap (OpenStreetMap Contributors 2020) or Global Administrative Areas (GADM) (Global Administrative Areas 2022). Examples of these differences are shown below in Figure 3-Figure 5.

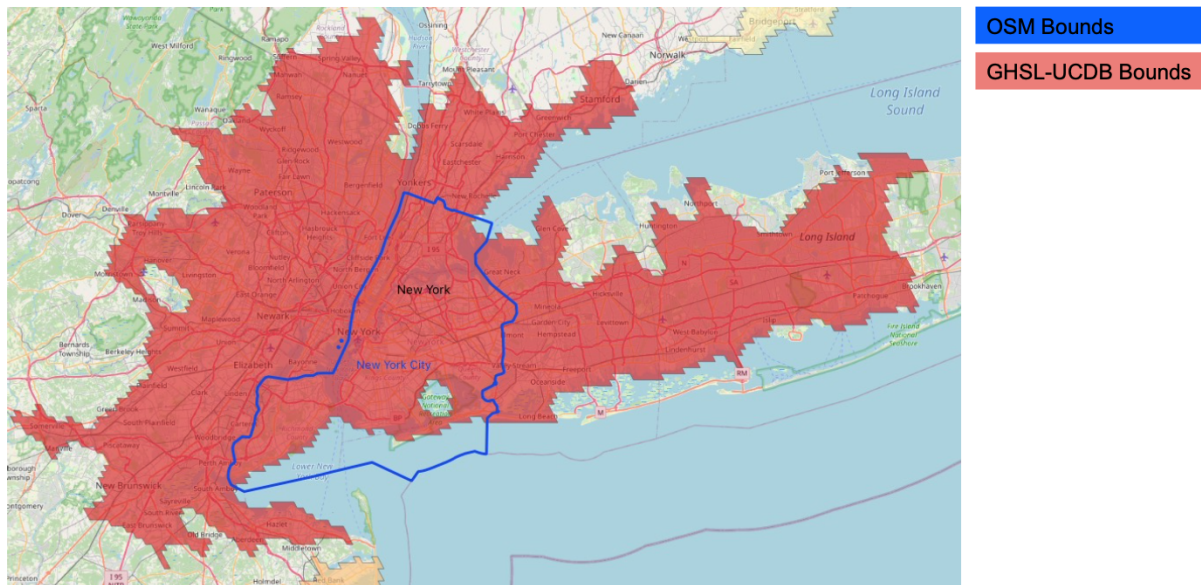


**Figure 3** Comparison of OSM administrative bounds (blue boundary) and GHSL-UCDB city bounds (red area) for New York City, USA

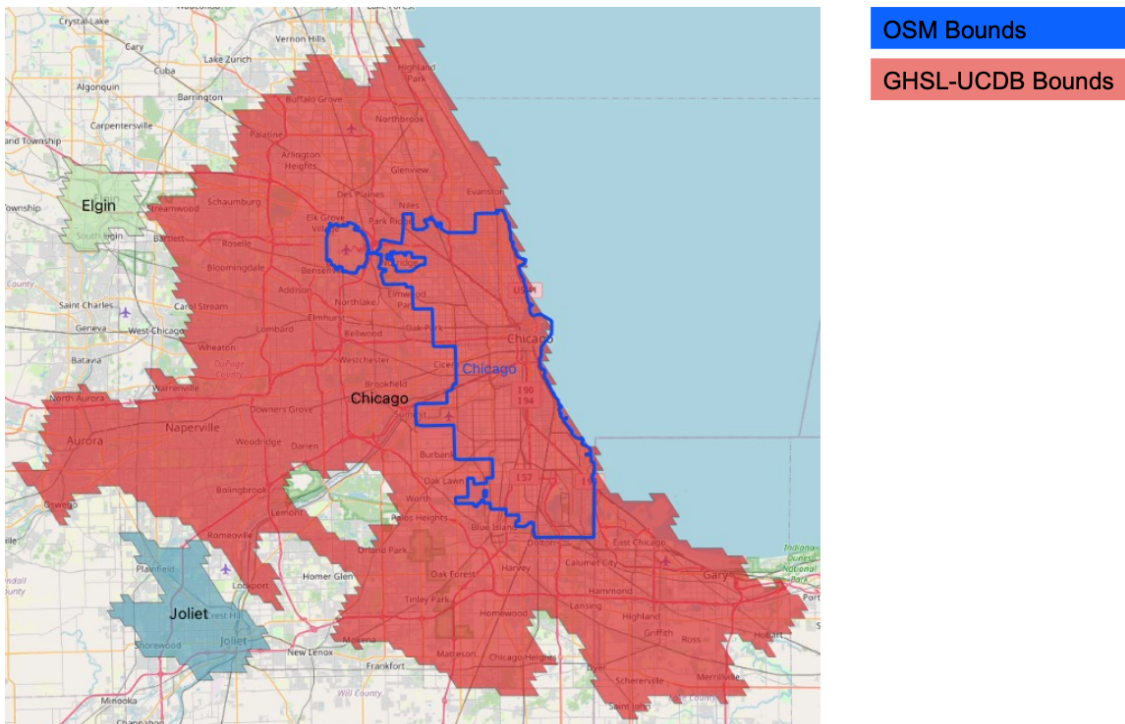


**Figure 4** Comparison of OSM administrative bounds (blue boundary) and GHSL-UCDB city bounds (red area) for Chicago, USA.

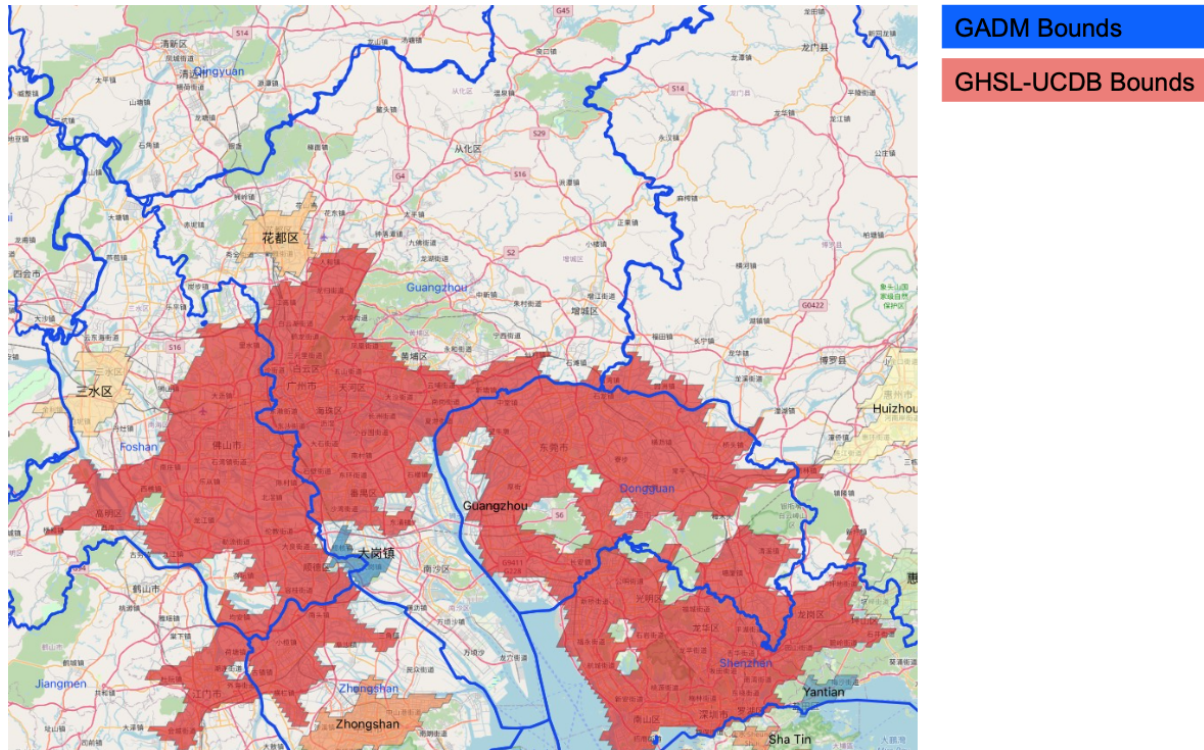


**Figure 5** Comparison of GADM level 2 administrative boundaries (blue boundaries) and GHSL-UCDB urban center bounds (red area) for Guangzhou, China.

UCDB spatially combines urban center bounds with a variety of associated metadata related to geography, socio-economic, environment, disaster risk, and sustainable development goals. This metadata includes EDGAR V5.0 emissions estimates within urban center bounds for 1975, 1990, 2000, and 2015 (Crippa et al. 2020). In last year's selection of 500 urban centers for Climate TRACE emission estimates, we relied on the EDGAR data to prioritize the centers. When looking at the full UCDB dataset, however, about 245 urban centers have invalid EDGAR transportation emissions; they are listed as "NAN". These urban centers are biased to the sub-Saharan Africa and South and South-East Asia regions; selecting 10k cities based solely on EDGAR emissions would therefore introduce an undesired bias; see Figure 6.

After first removing cities that do not pass the GHSL quality checks, urban areas were selected from the GHSL UCDB by selecting the 10k cities with the highest total built-up area in 2015 (field B15 in the database). This quantity represents the total building footprint area for a city and is expected to be reasonably correlated with transportation emissions. We specifically avoided the use of GHSL total resident population in 2015 (field P15) due to the possibility of significant outliers for smaller cities; see, for example, Figure 7.

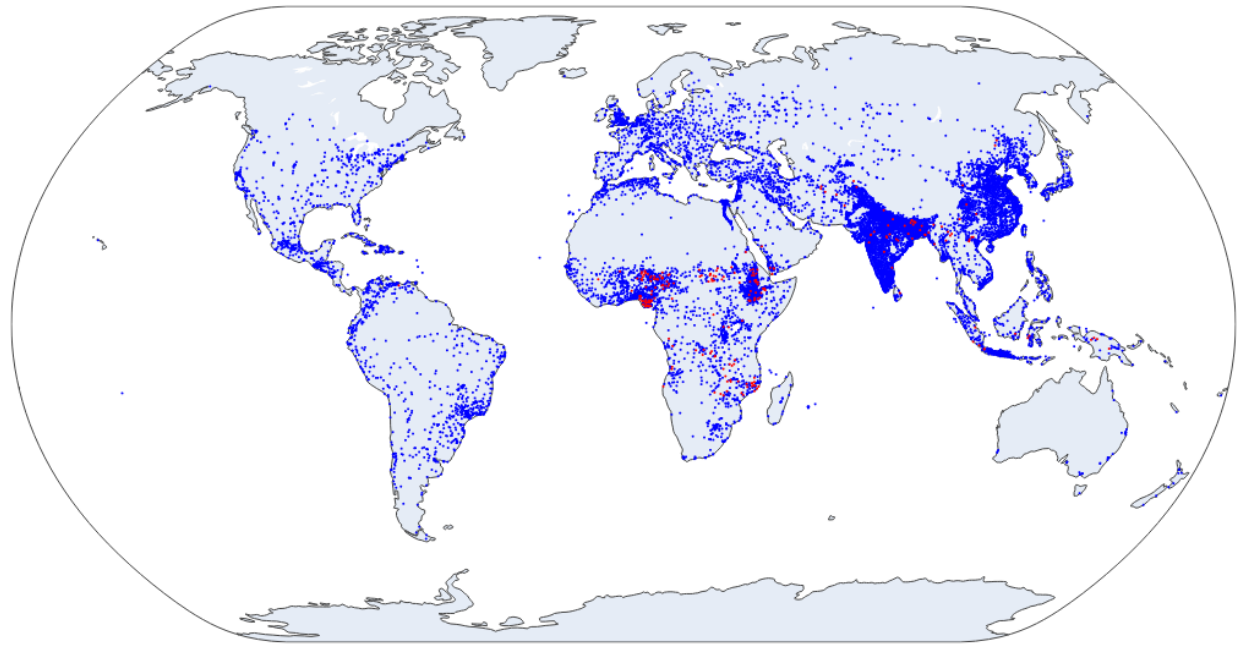


**Figure 6** Map of all GHSL UCDB urban centers (“cities”) with valid (blue) and invalid (red) EDGAR Emissions values.

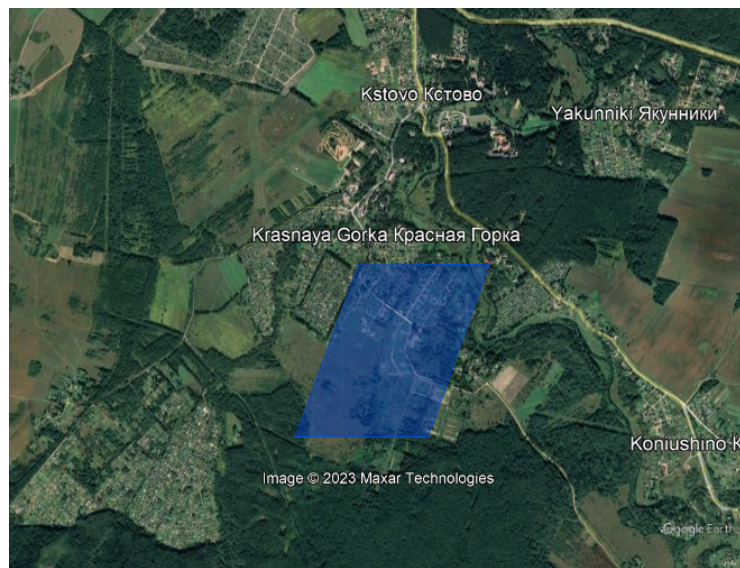


**Figure 7** Small  $1\text{km}^2$  “city” of Kstovo in rural Russia with GHSL-reported 2015 total resident population of 167k (blue area).

The distribution of the selected urban areas across continents is shown below in Table 1. Also shown for comparison is the previous distribution when only 500 urban areas were considered.

**Table 1** Comparison of regional representation of 500 and 10,000 urban areas using the EDGAR or the 2015 built-up area fields, respectively, from the GHSL UCDB data set.

Region	500 Urban Centers	10,000 Urban Centers
Asia	42.6%	58.29%
Africa	8.2%	16.69%
Europe	18.8%	10.56%
Latin America and the Caribbean	11.2%	10.30%
Northern America	17.8%	3.72%
Oceania	1.4%	0.44%

Due to how GHSL UCDB defines urban centers without reference to administrative boundaries, these centers can sometimes cross national borders. Out of the initial 10k urban centers, 135 cross at least one border. See for example the San Diego/Tijuana urban center in Figure 8. To avoid misattribution, the centers were divided along administrative boundaries; see the next section.

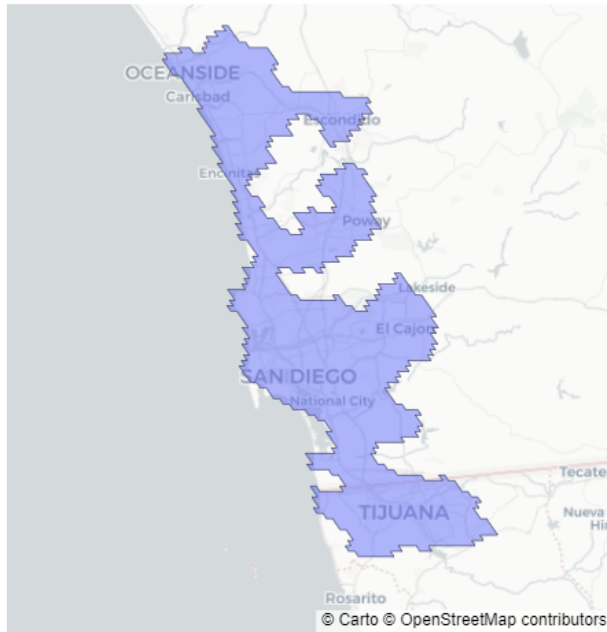


**Figure 8** Example of a GHSL UCDB urban area definition crossing national boundaries. Here, the definition of the “Tijuana” urban area encompasses several administrative cities, such as Tijuana in Mexico as well as San Diego and Oceanside in the USA.

### 2.2.2. Urban Area Administrative Boundaries

The Climate TRACE coalition decided to assign emissions based on Global Administrative Areas (GADM) (Global Administrative Areas 2022) at the country (Level 0) and county<sup>1</sup> (Level 2) levels. The coalition used a slightly modified version of GADM v4.1; details are described in Section 7.3. For the urban area dataset described above, this splits the 10,000 GHSL UCDB urban centers further. In large urban areas such as Tokyo (Japan), Guangzhou (China), or Los Angeles (USA), there might be up to nearly 200 Level 2 areas that intersect with the GHSL UCDB urban center. Our final dataset of urban areas therefore contains nearly 18,000 entries, formed from the intersection of a GADM Level 2 area with the GHSL urban center bounds.

### 2.2.3. Visual Satellite Imagery

Remote sensing imagery from the Sentinel-2A/B satellites were used as input data in our ML modeling approach to predict road transportation activity (see Section 2.3 below). The European Space Agency’s (ESA) Sentinel-2 mission comprises two satellites- Sentinel-2A, launched in 2015, and Sentinel-2B, launched in 2017 (Main-Knorn et al. 2017). Each Sentinel-2 satellite has a 10-day revisit time with a 5-day combined revisit. Both satellites are equipped with a multispectral (MSI) instrument which provides 13 spectral band measurements, blue to shortwave infrared (SWIR) wavelengths (~442 nm to ~2202 nm) reflected radiance. We used the

---

<sup>1</sup> “county” is the USA based English-version name of the typical administrative area. In other countries, other English-translated names are used.

Sentinel-2 Level-2A product at 10 m x 10 m resolution, using bands 4 (red), 3 (green), and 2 (blue) (Drusch et al. 2012).

#### 2.2.4. Road Network Data

Using the open-source tools Osmium (Jochen Topf 2023) and OSMnx (Boeing 2017) and custom filters, OpenStreetMap data for each city was cropped and filtered to the set of roads that carry normal vehicular traffic (see Section 2.2.6 below for details). A multi-directed graph of the road network was created from that data, and the total edge length (meaning the road length for each direction of traffic is counted separately) was computed to yield the reported road network length (in kilometers). Example road networks are visualized in Figure 9. A plot of road network length is provided in Figure 10; only the top 20 GHSL UCDB urban centers are displayed for visual clarity.

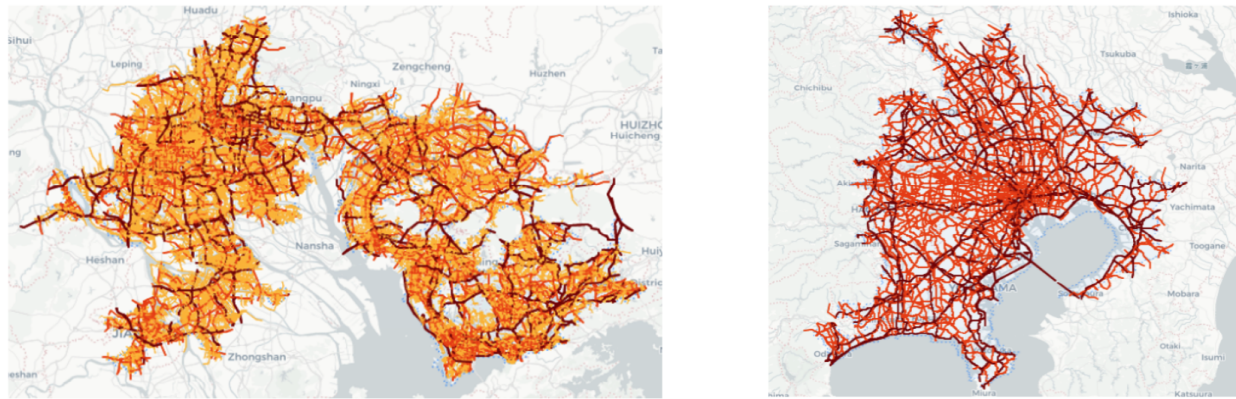


**Figure 9** Example road network data for Guangzhou, China (left) and Tokyo, Japan (right). Highways are in dark red, arterial roads in orange, and local roads in yellow. Local roads are intentionally not displayed for Tokyo due to their large count.

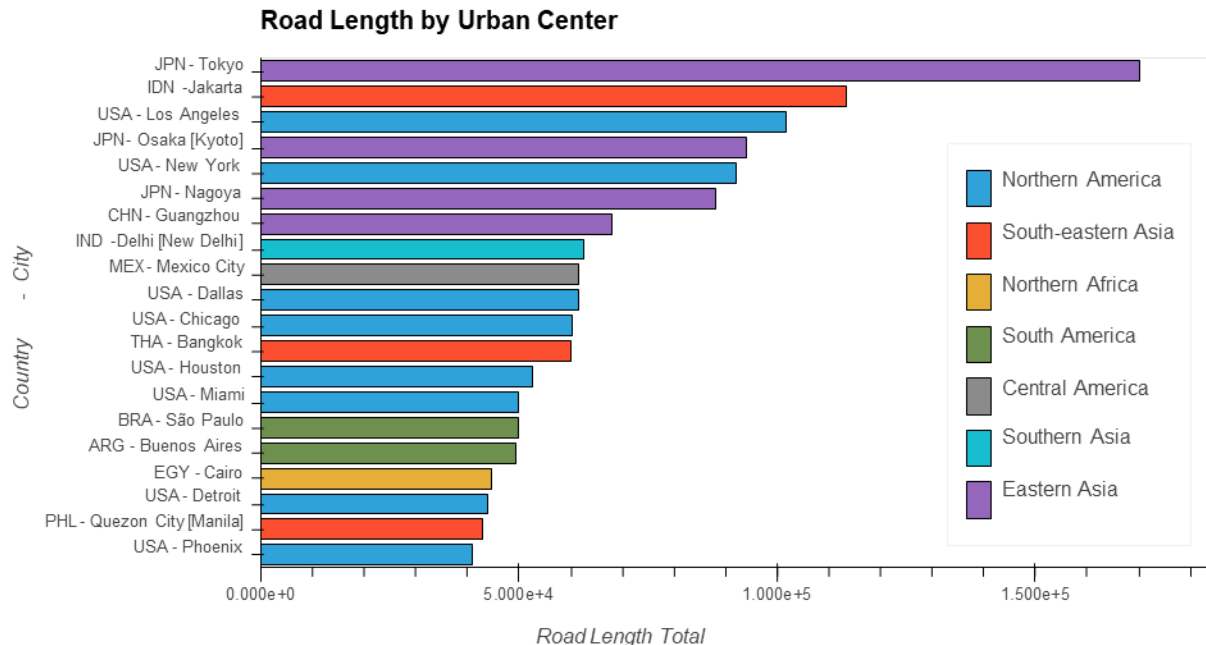


**Figure 10** Total road length for the top 20 GHSL UCDB urban centers (“cities”) colored by region.

Roads and associated metadata (including coordinates, number of lanes, etc.) are constantly changing around the world. OpenStreetMap is updated continuously in an attempt to keep an atlas that reflects reality. While most road segments are consistent between quarters, some road segments appear, some road segments disappear, and some have properties that change. We attempt to deal with these changes by using one snapshot of data from OpenStreetMap per quarter per year. For our activity and emissions estimates per road segment for a given year, we use model inference ensembling to combine four quarters of data; more details are given in Section 2.3.4.

### 2.2.5. Emissions Factors

Calculating emissions factors for an urban area was a complex process, due to the fact that an urban area can actually contain potentially hundreds of thousands of individual road segments, which might be considered “sub-sources”. Transportation emissions factors are dependent on many variables, including (but not limited to) road category, vehicle type, fuel type, and fuel efficiency. Data collection for each of these variables across 10,000 urban areas was a significant undertaking. Thus, the initial version of estimated emissions factors focused on collecting data at the country level for the 181 countries in which the urban areas were located. A detailed description of the urban area-level emissions factor calculation is provided in Section 2.2.10 below. Sources for each type of data required for the emissions factor calculation are shown below in Table 2, with descriptions of each data type provided in subsequent sections.

**Table 2** Primary emissions factors data sources used.

Data Type	Source(s)
Road Segment Type	OpenStreetMap (OpenStreetMap Contributors 2020), see Section 2.2.6 below
Vehicle Fleet Mix	Various, see additional information in Section 2.2.7 and Section 6.1
Fuel Type	CURB (World Bank Group 2019), see Section 2.2.8 below
Fuel Efficiencies	CURB (World Bank Group 2019), see Section 2.2.8 below
GHG Emissions Factors	U.S. EPA GHG Emissions Factors Hub (US EPA 2022), see Section 2.2.9 below

## 2.2.6. Road Segment Type

Road segment types (categories) were derived from OpenStreetMap data for all 500 cities. The current supported road types are highway, arterial, and local, which were chosen to align with other similar emissions inventories and traffic-related databases. The mapping between these road types and their respective OSM tags is provided in Table 3. Road type categorization is important in the emissions factor calculation for a given road segment as other emissions factors variables, including vehicle fleet mix and fuel efficiency, could vary significantly across different types of roads. These classes are also used within the modeling effort to distinguish roads (see Section 2.3.2).

**Table 3** Road segment type association with OpenStreetMap tags

Road Class	OpenStreetMap Tags
Highway	motorway, motorway_link, trunk, trunk_link
Arterial	primary, primary_link, secondary, secondary_link
Local	tertiary, tertiary_link, residential, living_street, unclassified

## **2.2.7. Vehicle Fleet Mix**

Vehicle fleet mix refers to the distribution of total vehicles in a given country across various vehicle types. The supported vehicle types were: passenger cars, light duty trucks, single unit trucks, combination trucks, motorcycles, and buses. Country-specific vehicle distribution numbers do not always share these same categories. There might be one, two or more country-specific categories mapping to one supported type or there might be no country-specific category that matches a supported type. These differences were dealt with on a per-country basis. For example, in countries which only reported “trucks” as a single category, we used regional averages of the percentage of trucks in each category to interpolate the single reported category into the three standard truck types.

In general, there are two categories of information available on vehicle fleet mixes: registration data and proportions of kilometers traveled by vehicle category. Our vehicle fleet mix encompasses both types of data and does not distinguish between them in accuracy.

For example, the US Federal Highway Administration (FHWA) provides estimates of both registered cars by state in Table MV-1 (US FHWA 2018) and vehicle-miles traveled in Table VM-4 (US FHWA 2020). These differ in the percentages of vehicles in each standard type. We would argue that the former (vehicle-miles traveled) is the better distribution of vehicle types to use, as we are attempting to estimate emissions from vehicles actually traveling on roads. However, we have not found such specific information for many countries. Instead, we use the following prioritized list to estimate the vehicle mix in each country:

1. Distribution of vehicle-km travelled categories: as described above
2. Distribution of registration types: as described above
3. Neighboring country average of vehicle fleet mix: use the average vehicle fleet mix from any countries whose GADM Level 0 border touches the target country
4. US FHWA estimate: when all else fails, use the US FHWA estimate for the USA

Country-specific vehicle fleet data was used for 103 countries. A full listing of the countries with country-specific data and their respective sources is provided in the supplementary material (see Section 6.1). Vehicle fleet mix values are currently the same across all supported road types but will be updated as sources of road type-specific data are identified.

## **2.2.8. Fuel Type and Efficiencies**

Due to the fact that different fuel types have different emissions factors, it is important to know the relative mix of fuel types for each type of vehicle traveling on a given road segment. The types of supported fuels are:

- Gasoline: no distinction is made between different sub-categories such as (in the US) 87, 89, and 91 octane gasoline or ethanol-free gasoline.

- Diesel: no distinction is made between sulfur-free diesel, bio-diesel or other sub-categories
- Compressed natural gas (CNG)
- Liquefied petroleum gas (LPG)
- Plug-in hybrid: no distinction is made between hybrids that run on different liquid fuels
- Battery electric vehicle (BEV)
- Other fuels (e.g., biogas, ethanol)

The primary source of this data is the Climate Action for Urban Sustainability (CURB) tool (World Bank Group 2019), which provides a global database of fuel type mix by country. Future updates may include updated country or city-specific fuel type data.

CURB was also the primary source of fuel efficiency data for all countries. CURB fuel efficiency values are reported in units of kilometers per liter and were extracted for all supported fuel and vehicle types described above. Fuel efficiencies were the same across all supported road types (highway, arterial, and local) in this release, but may be continuously updated as better country or city-specific datasets are located.

### **2.2.9. Vehicle Greenhouse Gas (GHG) Emissions Factors**

GHG emissions factors refer to how much of a given gas is emitted per unit of fuel burned and varies by fuel type. Our data focuses on carbon dioxide (CO<sub>2</sub>), nitrous oxide (N<sub>2</sub>O), and methane (CH<sub>4</sub>) emissions factors, using data from the U.S. Environmental Protection Agency (US EPA 2022).

For nitrous oxide and methane, the emissions factors for each gas were given in units of grams of each gas per mile driven. This was different from the data for carbon dioxide, which was given as grams per liter. To normalize all greenhouse gas emissions factors to “grams per liter”, we used fuel efficiency data (given in “liters per km”) to generate data for nitrous oxide and methane as grams per liter.

### **2.2.10. Road Segment Type Emissions and Emissions Factors**

Total emissions were first computed for each road segment within an urban area, and then summed to estimate total city emissions (CE) for each greenhouse gas  $g$ :

$$CE_g = \sum_i SE_{g,i} \quad (1)$$

where  $SE_{g,i}$  is the “segment emissions” for a road segment  $i$ . Each  $SE_i$  was calculated as:

$$SE_{g,i} = 365 \cdot AADT_i \cdot l_i \cdot \sum_{v,f} \eta_{v,f,s_i} \cdot m_{v,f,s_i} \cdot g_{v,f,s_i} \quad (2)$$

where:

- 365 is the days in a year (kept constant across any and all leap years),
- $AADT_i$  is the average annual daily traffic (unitless vehicles) of the road segment  $i$ .
- $l_i$  is the length of the road segment  $i$ , in units of km (see section 2.2.4),
- $\eta_{v,f,s_i}$  is the fuel efficiency, in units of liters per km (see section 2.2.8), for a vehicle type  $v$ , fuel type  $f$  and a road segment category  $s_i$  of the road segment  $i$ ,
- $m_{v,f,s_i}$  the vehicle mix (see section 2.2.7), as a fraction, typically present on the road segment based on the vehicle type  $v$ , fuel type  $f$  and a road segment category  $s_i$  of the road segment  $i$ . Specifically, we require that  $\sum_{v,f} m_{v,f,s_i} = 1$  for each road segment category  $s_i$ . See Table 3 for allowed road segment categories.
- Finally,  $g_{v,f,s_i}$  is the greenhouse gas emissions factor (see Section 2.2.9), in grams of gas per liter, for the vehicle type  $v$ , fuel type  $f$  and a road segment category  $s_i$  of the road segment  $i$ .

All three of  $\eta_{v,f,s_i}$ ,  $m_{v,f,s_i}$ , and  $g_{v,f,s_i}$  are look-up tables based on data gathered from several sources. A list of supported road segment types is provided in section 2.2.6, supported vehicle types in section 2.2.7, supported fuel types in section 2.2.8, and greenhouse gas factors in 2.2.9. We calculated separate CEs for every greenhouse gas, and used IPCC GWP20 and GWP100 values (Forster, P. et al. 2023) to convert methane and nitrous oxide emissions into carbon dioxide equivalent emissions.

To calculate a city emissions factor (CEF), we calculated the total city emissions and divided by the total activity, defined as the sum over all road segments of the AADT times length for each segment:

$$CEF_g = \frac{CE_g}{365 \cdot \sum_i AADT_i \cdot l_i}. \quad (3)$$

As with the CE calculation, we calculate a separate CEF for each of the three major greenhouse gases. Thus, three emissions factor values were provided for each city, representing the average amount of each greenhouse gas emitted per kilometer traveled by a single vehicle on any road segment within that city. The units of each provided city emissions factor (CEF) are metric tons (tonnes) of greenhouse gas per vehicle kilometer traveled (VKT).

## **2.3. Machine Learning Models**

As part of our hybrid modeling approach, machine learning (ML) models were trained to estimate road activity from satellite imagery and road network data. These estimates were required in the absence of global, openly available, and high-quality traffic activity data and is a significant departure from existing methods.

### **2.3.1. Ground Truth Road Activity Data**

To train our ML models, we utilized the U.S. Highway Performance Monitoring System Average Annual Daily Traffic (AADT) data from 2017 and 2018 (US FHWA 2017). This AADT data was recorded using road-side devices and was provided by each state independently. We utilized the total AADT measure in our work, measured in vehicles per day. AADT data was not available for every road segment and was typically only recorded on major highways and arterial (collector) roads.

### **2.3.2. Convolutional Neural Network (CNN)**

Our first machine learning approach used semantic segmentation CNNs to predict AADT. Specifically, we input visual satellite imagery in combination with rasterized road network data to predict AADT on a per-pixel basis (Figure 12). This approach was informed by previous work in directly regressing road transport CO<sub>2</sub> emissions (Mukherjee et al. 2021). Models were trained using the Sentinel-2 Level-2A product at 10 m x 10 m resolution, using bands 4 (red), 3 (green), and 2 (blue) (Drusch et al. 2012).

Road network data was retrieved from OpenStreetMap and rasterized for the corresponding extent of each visual image tile. Each standardized road type (*highway*, *secondary*, *local*, see Sections 2.2.4 and 2.2.6) was rasterized independently, and the resulting raster channels are concatenated together to form a three-channel image. This image was then combined with the visual image to form a six-channel input image that was input to the CNN. Thus, the CNN model is tasked with predicting the number of vehicles traveling on a road segment as a function of visual satellite image features and road location and type information. We primarily used MAnet-based architectures (Fan et al. 2020) for our segmentation models, based on the findings of similar previous work (Mukherjee et al. 2021).

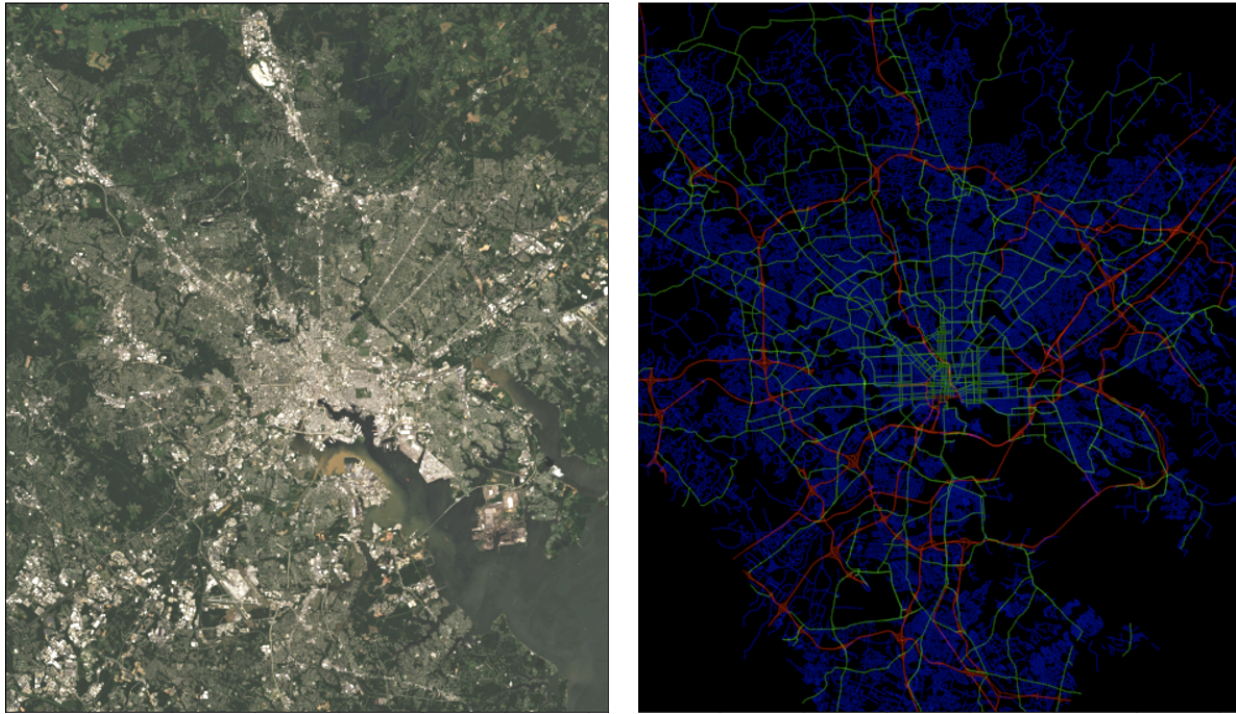


**Figure 11** Example Sentinel-2 visual (RGB) satellite image (left) and corresponding rasterized OSM road network data (right) for Baltimore, Maryland USA. The OSM raster colors represent different road types: highways (red), secondary roads (green), and local roads (blue).

When the model was used within the overall emissions calculation pipeline, pixel-based AADT predictions were post-processed to associate predicted values with their corresponding road segment. All AADT predictions for a given road segment were averaged to produce a single AADT value for that road segment across the geographic extent. A road ID to predicted AADT mapping was then saved and fed to the emissions factors pipeline for emissions calculation and aggregation, as described in Section 2.2.10.

### 2.3.3. Graph Neural Network (GNN)

Another type of ML model trained to predict AADT was graph neural networks (GNNs) (Bronstein et al. 2017). Road networks inherently take the form of a graph structure, and GNNs can capture road activity across a range of scales more easily than the image-based convolutional neural network (CNN) segmentation models. CNN-based solutions constrain the spatial area that can be covered during inference, making it difficult to capture potential dependencies on features in neighboring or distant locations. GNNs can easily leverage various features assigned to nodes and efficiently reason over the full road network graph to provide more robust estimates of on-road activity.

For this work, a GNN was trained using OpenStreetMap road network data, including a number of road features: the number of lanes, road length, road type, link or not (such as an exit ramp), and the directional angle between roads. The Graph Attention (GAT) network (Veličković et al.

2018) architecture was used as it allows for both edge and node input features, and was set up to predict log-AADT values. We note that the GNN does not use visual imagery as input and is able to learn a relationship between road types and configurations to the density of traffic on those roads.

#### 2.3.4. Model Training

Training data was increased in scope and normalized for temporal consistency between the US HPMS AADT ground truth and the OpenStreetMap road networks. Table 4 shows the details of the various data sources used for training a single GNN and CNN model.

**Table 4** Training details and comparison between the 2022 and 2023 release of the road transportation emissions datasets

Model	Training Data	2022 Dataset	2023 Dataset
GNN	<i>US HPMS AADT</i>	2017	2017 and 2018
	<i>OpenStreetMap Dataset Date</i>	January 23, 2022	4 quarters each in 2017 and 2018
	<i>Urban areas</i>	81 for training & validation; total 81 samples	308 areas for each quarter of 2017, and 307 areas for each quarter of 2018; total 2460 samples
	<i>US HPMS AADT</i>	2017	2017 and 2018
CNN	<i>Sentinel-2 Imagery</i>	Summer 2017; 3558 total images	One image per urban area, per quarter for a total of 2028 images
	<i>OpenStreetMap Dataset Date</i>	January 23, 2022	4 quarters each in 2017 and 2018
	<i>Urban areas</i>	1118 urban areas	308 areas for each quarter of 2017, and 307 areas for each quarter of 2018; total 2460 samples

With the CNN model training, we also changed the loss function used in training. In the 2022 dataset, we used a linear loss between *all* known roads (whether highway, arterial, or local) and

the ground truth AADT. However, not every road has measured AADT values (see Figure 13); in these cases, the model was erroneously being directed to infer zero AADT for those road segments. This resulted in the inferred AADT values for all roads, but especially minor roads, being much lower than desired.

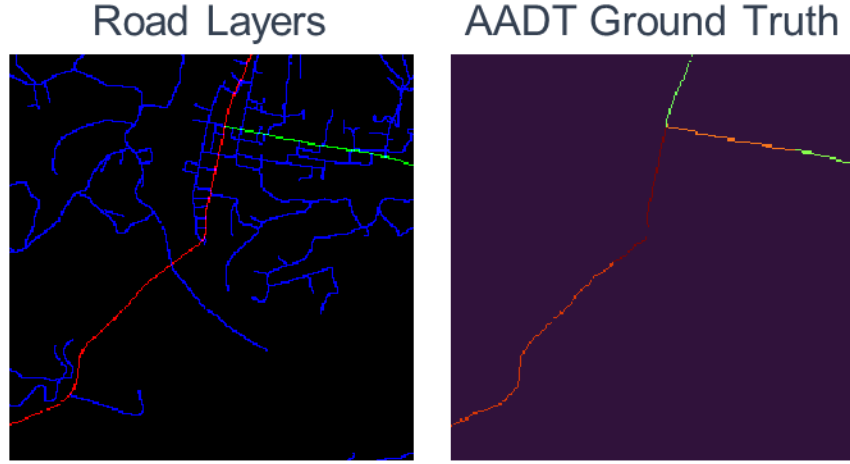


**Figure 12** Left: Red lines are highways, green lines are arterial roads, and blue lines are local roads. Right: the highway and arterial road in the above image both have nonzero AADT values, however the local roads all have zero AADT values.

The identified issue was addressed by applying a mask to the loss function where loss was only calculated when the AADT truth value was nonzero. These had the end result of bringing the GNN and CNN models much closer in agreement. The loss was changed from a straight Mean Square Error (MSE) loss term to a Mean Square Log Error term, to better match AADT values for smaller roads which are underrepresented in the HPMS data.

An additional semi-supervised loss term was added to account for the reduced constraint introduced by only including loss from where AADT was nonzero. For this loss term, the same image is passed through the model multiple times using different flips/rotations, and the loss then seeks to reduce the variance between the pixel level AADT estimates after undoing those flips/rotations.

### 2.3.5. Model Inference & Ensembling

The data sources for inference also changed slightly to take advantage of the greater number of trained models as described in Section 2.3.4. In Table 5 we highlight the differences between the 2022 dataset release and the current 2023-year data release.

**Table 5** Inference details and comparison between the 2022 and 2023 release of the road transportation emissions datasets

Model	Inference Data	2022 Dataset	2023 Dataset
GNN	<i>OpenStreetMap Dataset Date</i>	January 23, 2022	4 quarters each in 2021 and 2022
CNN	<i>OpenStreetMap Dataset Date</i>	January 23, 2022	4 quarters each in 2021 and 2022
	<i>Sentinel-2 Imagery</i>	Images from each season for 2021; a single season was chosen that reduced cloud cover	Image mosaics created from multiple images within each quarter matching OpenStreetMap data; road segments chosen that reduced in multiple images averaged together

For each urban area, for each year, we ended up with eight estimates of AADT for every road segment. However, as discussed in Section 2.2.4, OpenStreetMap data is continuously updated, and so not every road-segment is present across all eight estimates (four from the CNN, four from the GNN). Additionally, some CNN estimates were not possible due to persistent cloud cover (which we believe is an artifact of the Sentinel-2 revisit timing). To create a more robust and predictive AADT estimation model, ensembling was performed using the CNN and GNN models.

To ensemble the eight, possibly non-identical, sets of road-segment AADT predictions, we employed the following routine:

1. Concatenate the CNN and GNN road segment data for the same quarter-year
2. Group by the unique road segment ID, and take the average;

For cases where a road is only present in the GNN due to clouds in the CNN image, this effectively sets the data for that segment to the GNN predicted value

3. Concatenate the four quarters of data, and group by the unique road segment ID, followed by summing all data and dividing by 4.

As opposed to an average, this effectively weighs the road segments that only appear in one quarter as contributing lower to our estimate of emissions than road segments that are present in all four quarters.

An example ensemble AADT output can be seen below in Figure 14.

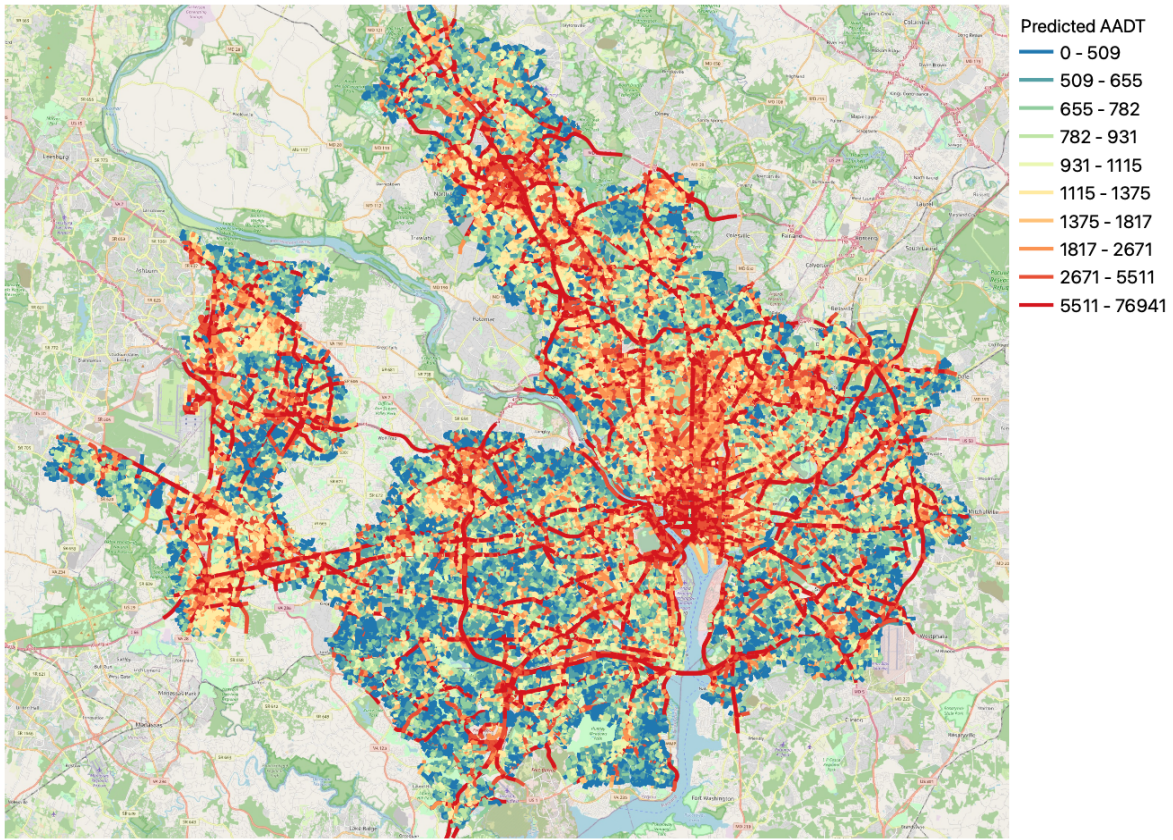


**Figure 13** Ensemble-predicted AADT for 2021, measured in vehicles per day, for Washington, D.C.

## 2.4. Uncertainty & Confidence

This dataset release also includes a first estimate of the uncertainty in our emissions estimates along with a confidence level for that uncertainty. In this section, we discuss our method for calculating an urban-area specific uncertainty along with known improvements that will be implemented in future dataset releases. Due to standardization across the entire Climate TRACE coalition, we estimate a standard deviation value; we are aware that our emissions estimates are not normally distributed and a standard deviation is insufficient to describe our uncertainty.

### 2.4.1. Uncertainty Overview

In addition to CO<sub>2</sub>, N<sub>2</sub>O, and CH<sub>4</sub> emissions estimates, we also provide estimates of activity (as defined in Section 2.2.10), capacity, and other values. A full dataset description is in Section 6.2. In Table 6 below, we summarize the approach taken to estimate the uncertainty in each value.

**Table 6** Summary of methods to estimate uncertainty per column

	Estimate from <a href="https://github.com/microsoft/RoadDetections">https://github.com/microsoft/RoadDetections</a>
capacity	
activity	Estimate for AADT, propagation of error from capacity
CO2_emissions_factor	Propagation of error from CO2 emissions and activity
CH4_emissions_factor	Propagation of error from CH4 emissions and activity
N2O_emissions_factor	Propagation of error from N2O emissions and activity
other_gas_emissions_factor	Propagation of error from other_gas_emissions and activity
CO2_emissions	Estimate from regional normalized spread of values
CH4_emissions	Estimate from regional normalized spread of values
N2O_emissions	Estimate from regional normalized spread of values
other_gas_emissions	Estimate from regional normalized spread of values
total_CO2e_100yrGWP	Propagation of error from CO2_emissions, CH4 emissions, and N2O emissions, including constants
total_CO2e_20yrGWP	Propagation of error from CO2_emissions, CH4 emissions, and N2O emissions, including constants

In the following subsections, we provide details on the estimation process in detail.

#### 2.4.2. Capacity Uncertainty

Capacity is simply defined as the total length of the road network in an urban area. We use OpenStreetMap, which is a global initiative with crowd-sourced data, to estimate the capacity. There are many urban areas around the world for which OpenStreetMap data does not match the apparent road network. To estimate the possible overall road-network error, we used the work by Microsoft Bing Maps (Microsoft Bing Maps 2023). To estimate a standard deviation across the whole world, the missing road lengths were divided by the total road length for each set of areas that both values were available to create a list of fractions corresponding to the missing percentage. A standard deviation of 2% missing roads was then calculated from this set of data. To calculate the urban area level error, we assumed that:

$$\frac{\sigma_{CAP}}{CAP} = \sigma_l = 0.02$$

Such that  $\sigma_{CAP} = 0.02 \cdot CAP$  and we report  $\sigma_{CAP}$  for the capacity of each urban area source.

In later uncertainty calculations, we require an estimate of the per-road-segment capacity error. We simply assume that the 2% error is set appropriately to sum up to the correct error estimate. To do so, we set the per-segment standard deviation  $\sigma_{l_i}$  to:

$$\sigma_{l_i} = \frac{\sigma_l}{\sqrt{\sum_i l_i^2}} CAP l_i = \sigma_l' l_i$$

where  $l_i$  is the length of each road segment. This results in the same value for  $\sigma_{CAP}$  when calculated using propagation of errors for sums:

$$\sigma_{CAP} = \sqrt{\sum_i \sigma_{l_i}^2} = \sqrt{\sum_i (\sigma_l' l_i)^2} = \sqrt{\sigma_l'^2 \sum_i l_i^2} = \sigma_l' \cdot \sqrt{\sum_i l_i^2} = \frac{\sigma_l}{\sqrt{\sum_i l_i^2}} CAP \cdot \sqrt{\sum_i l_i^2} = \sigma_l \cdot CAP.$$

### 2.4.3. Activity Uncertainty

Recalling that

$$ACT = 365 \cdot \sum_i AADT_i \cdot l_i$$

we can estimate the standard deviation of the activity as being due to the standard deviation in the length of the segment (as in the capacity discussion above) and the standard error of the AADT estimate. We assume explicitly that the per-segment AADT estimate has some constant percent error  $\sigma_a$ :

$$\sigma_{a_i} = \sigma_a a_i$$

such that

$$\sigma_{ACT} = 365 \cdot \sqrt{\sum_i \left( l_i^2 \sigma_{a_i}^2 + a_i^2 \sigma_{l_i}^2 \right)} = 365 \cdot \sqrt{\left( \sigma_a^2 + \sigma_l'^2 \right) \sum_i (l_i a_i)^2}$$

By comparing the ground truth AADT values per segment and the corresponding ensembled annual average, we estimate

$$\sigma_a = 0.56.$$

In estimating the activity error, there is a simplifying assumption that per-segment AADT errors are independent; this is not expected to actually be the case, and per-segment AADT errors are likely correlated due to the ML models.

### 2.4.4. Emissions Uncertainty

There are three different gases for which we estimate uncertainty in the same way. We have decided to report the uncertainty in our emissions estimate as an estimate of the variability in our final estimates, which may come from many known and unknown sources. It should not be

interpreted as an error relative to a ground truth, which does not exist. Instead, it should be understood as an estimate of self-consistency in our own datasets.

To estimate this variability and self-consistency, we use the following routine:

1. Group urban-areas into regions as specified by official UN Regions (we combine “Micronesia” and “Melanesia” into a single “Melanesia” region due to the small number of urban areas in Micronesia).
2. Use the CO<sub>2</sub> emissions as source of estimates since it is the largest contributor to total CO<sub>2</sub>e
3. Calculate an area- and median-normalized emissions per urban area  $j$ :
  - a. First, normalize by area (in km) of the urban area:

$$E_{j,a} = \frac{E_j}{area_j};$$

we treat area as error-less and preferable in this normalization over something like capacity. Here  $E_j$  is the emissions estimate for the urban area  $j$ .

- b. Second, normalize by the median:

$$E_{j,a-m} = \frac{E_{j,a}}{\text{median}(\{E_{1,a}, E_{2,a}, \dots, E_{k,a}\})} - 1$$

this normalization creates a dimensionless value for which a distribution is centered on 0

4. From the distributions of area-median-normalized emissions  $E_{j,a-m}$  for each region, calculate the probability percentiles for these emissions within a region
5. Convert percentile distributions to a standard deviation for  $E_j$ :
  - a. Find the lower and upper bounds of normalized emissions by using the 16<sup>th</sup> and 84<sup>th</sup> percentiles:  $\{\delta E_l, \delta E_u\}$  – this is equivalent to the  $\pm\sigma$  in a normalized distribution
  - b. Since these are normalized percentiles centered on 0,  $\delta E_l < 0, \delta E_u > 0$
  - c. Calculate, per UN region  $r$ ,  $\sigma_r = \frac{\delta E_u - \delta E_l}{2}$
6. Apply the normalized standard deviation to each raw emissions value:

$$\sigma_{E_j} = \sigma_r E_j$$

#### 2.4.5. Emissions Factors Uncertainty

Having calculated the emissions uncertainty  $\sigma_{E_j}$ , we can calculate the emissions factor (defined as  $E_j/ACT_j$ ) via the propagation of error:

$$\sigma_{EF_j} = \sqrt{\left(\frac{E_j}{ACT_j}\right)^2 \left( \frac{\sigma_E^2}{E_j^2} + \frac{\sigma_{ACT_j}^2}{ACT_j^2} \right)}$$

This process can be repeated for each of the three gases reported.

#### 2.4.6. Total Equivalent CO<sub>2</sub>: 20 and 100 Year Baselines

These two columns are calculated from propagation of error of the total:

$$TOT_z = CO2 + CH4 \cdot CO2e_{CH4,Z} + N2O \cdot CO2e_{N2O,Z}$$

Where  $Z \in \{20, 100\}$  are the two different baselines,  $CO2e_{CH4,Z}$  is the equivalent CO<sub>2</sub> emissions for methane, and  $CO2e_{N2O,Z}$  the equivalent CO<sub>2</sub> emissions for nitrous oxide. We use the propagation of error along with the standard IPCC definitions of error in the equivalent CO<sub>2</sub> emissions such that:

$$\sigma_{TOT_z} = \sqrt{\sigma_{CO2}^2 + CH4^2 \sigma_{CO2e_{CH4,Z}}^2 + CO2e_{CH4,Z}^2 \sigma_{CH4}^2 + N2O^2 \sigma_{CO2e_{N2O,Z}}^2 + CO2e_{N2O,Z}^2 \sigma_{N2O}^2}$$

#### 2.4.7. Confidence

As described above, there are many assumptions and rough approximations made in order to estimate a standard deviation of many different parameters calculated from our models. We judge, based on subject matter expertise and knowledge that this initial calculation is inadequate, that all uncertainty parameters calculated here have a LOW confidence using standard IPCC confidence ranges.

### 2.5. International Emissions Inventories

Comparison against one international emissions inventory has been performed for the global 10,000 GHSL UCDB urban centers using EDGAR v7.0 (Crippa et al. 2020). EDGAR provides a global inventory for transportation that uses road density as a proxy to spatially distribute emissions. Other possible inventories, such as Google EIE or Carbon Monitor, for example, do not have open data sources that we could easily download across our entire dataset. Additionally, the methodology and bounds used by those approaches do not coincide with our urban center definitions. As a public, gridded product, the EDGAR dataset is somewhat more amenable to comparisons against our datasets.

Our emissions estimates are compared against EDGAR v7, both within the USA and globally. This comparison is performed for initial validation of our data; it is not used for uncertainty estimates. There are significant differences between the way EDGAR v7 data is reported and the way we calculate emissions. EDGAR v7 uses a grid across the entire world to report CO<sub>2</sub> emissions, while we use geographic bounds based on GHSL and GADM boundaries (see Section 2.2.2). In many cases, the density of urban centers is such that multiple centers are present in a single “cell” of EDGAR data (see Figure 21).

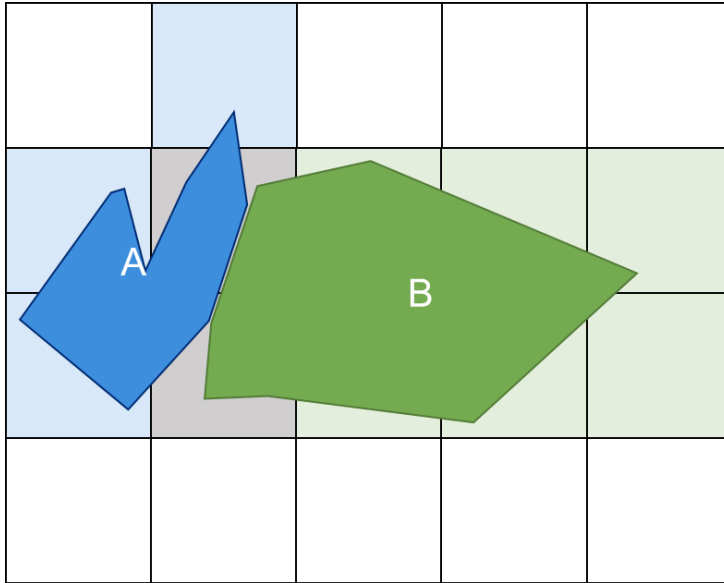


**Figure 14** Diagram of EDGAR unit-cells on a geographic grid compared with two different urban centers with geographic extents.

To provide a consistent estimate across the two datasets, we use the following routine (see Figure 21 for a visualization):

1. Use emissions from the same GHSL urban center (by combining all emissions from that center split across GADM-based urban areas)
2. Find all EDGAR squares which overlap the GHSL urban center geographic extents
3. Sum all short and long cycle CO<sub>2</sub> emissions from those squares
4. Each GHSL area (e.g., “A” and “B”) is treated *independently*: both EDGAR estimates for “A” and “B” will include all emissions from the grey boxes, for example
5. The resulting estimate from EDGAR is compared to the GHSL urban center estimate

See Section 3.3 for a discussion of the results of the comparison.

### 3. Results

In this section, we highlight top-level trends and differences between dataset release years. Specific information on per-urban-area emissions is available in the released dataset.

#### 3.1. Machine Learning Model Ground Truth Comparison

While each trained ML model reduces the difference between the ground truth AADT values and the inferred values, it is worthwhile comparing a visual representation of the kinds of differences we see. In Figure 15 and Figure 16 below, we show a hexbin plot of predicted vs ground truth AADT values for the CNN Model, the GNN Model, and the ensemble for both the 2023 dataset release (Figure 15) and last years’ 2022 dataset release (Figure 16).

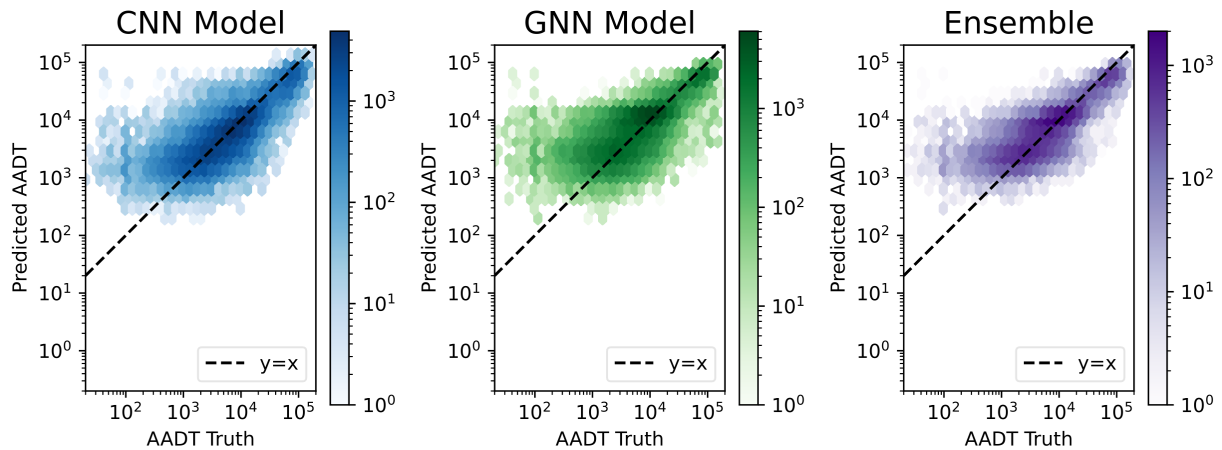


**Figure 15** 2023 Dataset release year comparison of predicted AADT vs. ground truth across a set of 14 test cities in the US.

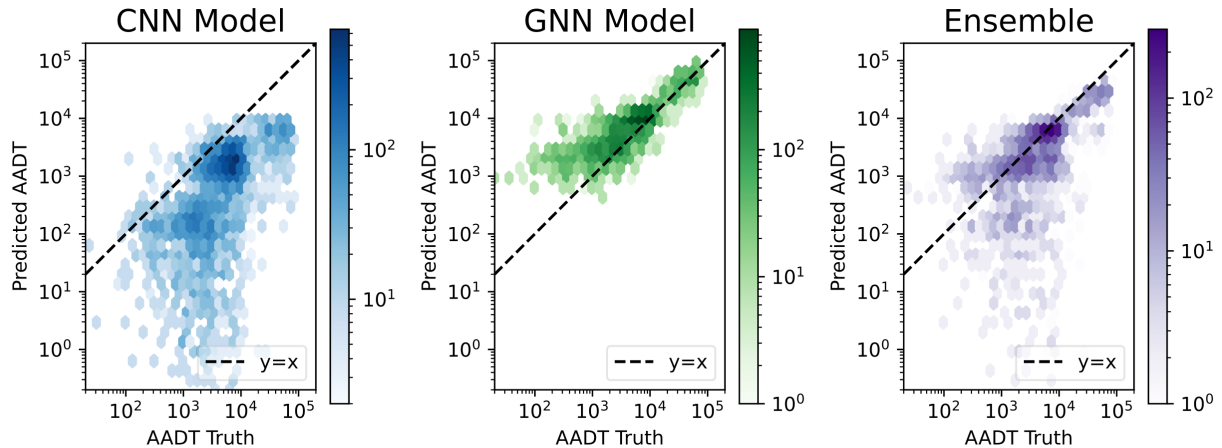


**Figure 16** 2022 Dataset release year comparison of predicted AADT vs. ground truth across a set of 14 test cities in the US.

The dashed lines in the plots indicate the line along with predicted and ground truth AADT values are equal. Bins within the plot that have a darker color are places which have more instances in that bin according to the color scale presented. Note that there is a much larger number of data points underlying the 2023-year results due to there being 8 quarters of road networks and truth data, as opposed to only one, effectively, for the 2022 data.

Comparing the “CNN Model” plots in Figure 15 and Figure 16, we find that the 2022 predictions were significantly underestimating the AADT values for all roads, which is no longer the case in 2023 predictions. In fact, across both CNN and GNN models in 2023 there is a tendency for roads to overestimate AADT values for lower trafficked roads (with AADT truth value less than  $10^{3.5}$ ) and underestimate the AADT values for highly trafficked roads (with AADT truth value greater than  $10^{3.5}$ ).

This significant increase in the predicted AADT values across all road segments of the 2022 CNN models led to an increase of approximately 77% in the predicted emissions for nearly 500 cities in the 2023-dataset emissions estimates compared to the 2022-dataset emissions data. Figure 17 below shows the comparison between the two dataset release dates. In the 2023 dataset release, we estimated emissions for two calendar years (2021 and 2022) while in the 2022 dataset release, we only estimated emissions for one calendar year (2021). The blue line shows the trend expected if the total CO<sub>2</sub>e was constant between the two dataset releases.

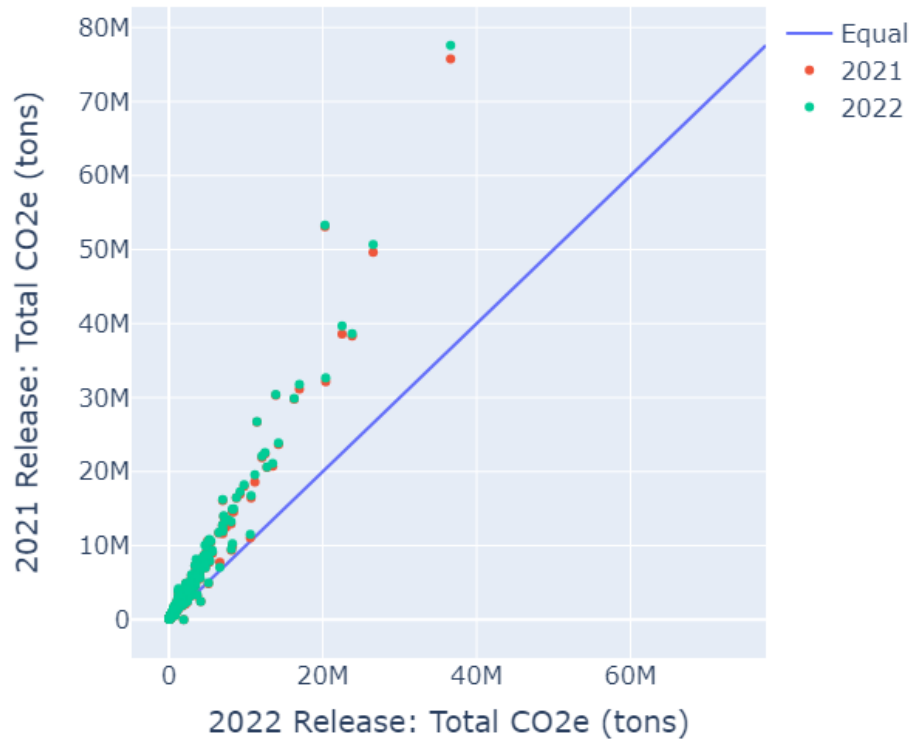
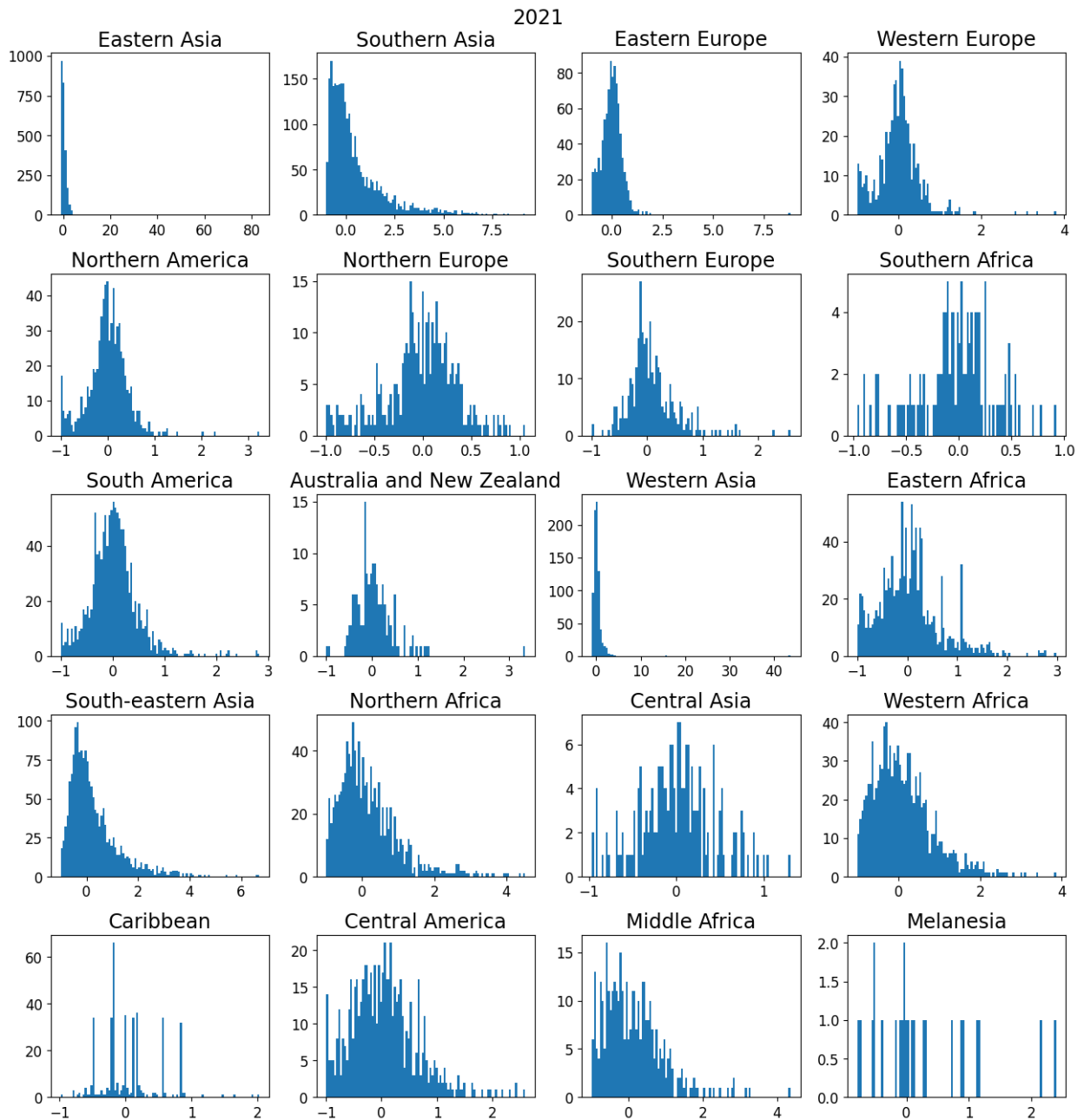


**Figure 17** Comparison of the common 500 urban areas between the 2023 and 2022 dataset releases.

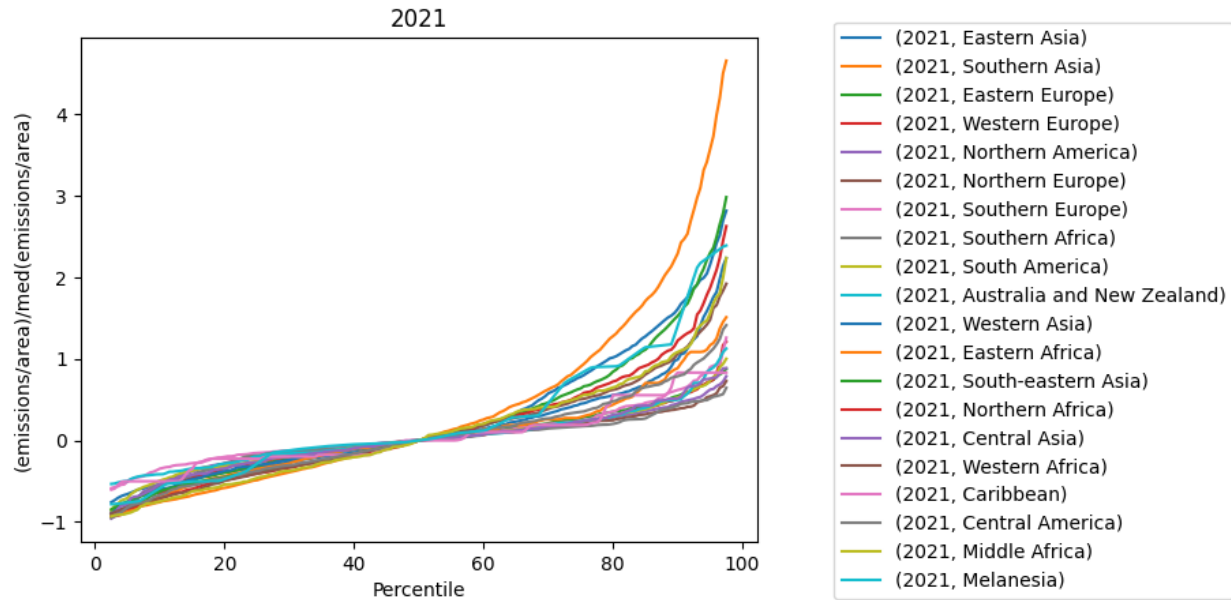
### 3.2. Emissions Uncertainty

Figure 18 and Figure 19 below show the results of steps 3 and 4, respectively, of the methodology described in section 2.4.4. It is clear from these distributions that very rarely are the histograms normally distributed.

In we show the value of  $\sigma_r$  across all regions.



**Figure 18** Area- and median-normalized emissions histograms per region for emissions estimates in 2021 after step 3 of the routine described in text.



**Figure 19** Percentile distribution of area-median-normalized emissions per region after step 4 of the routine described in text.

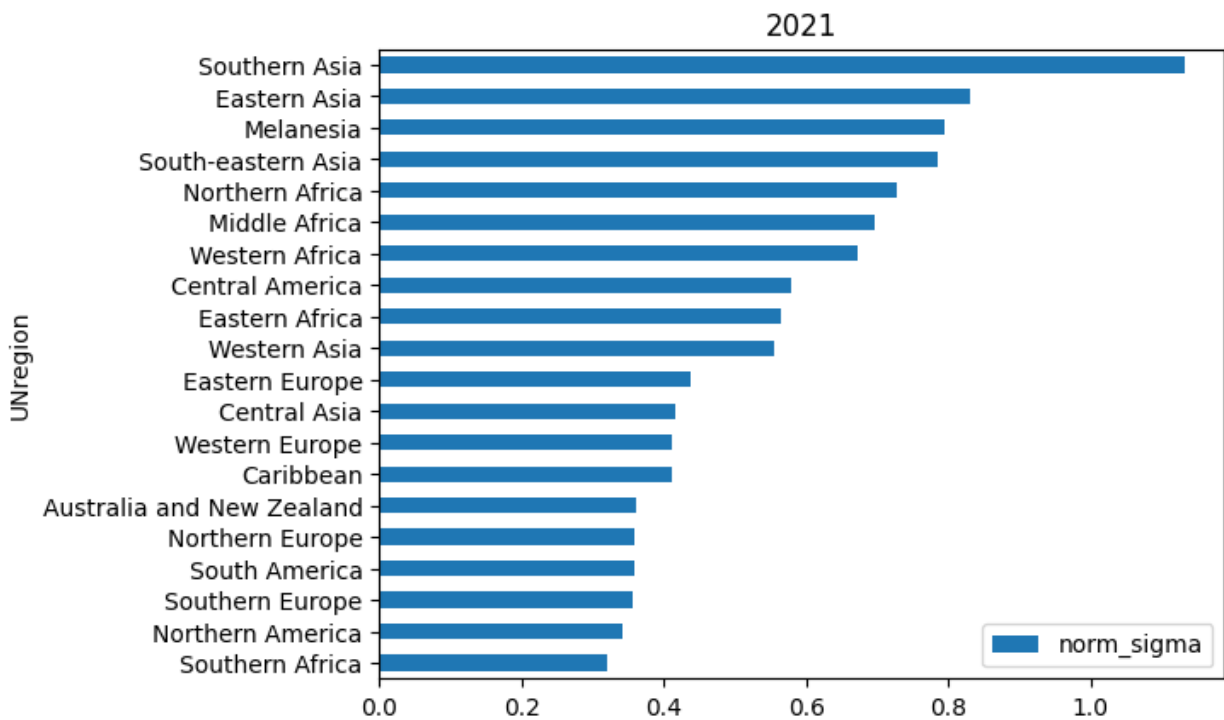


**Figure 20**  $\sigma_r$  as calculated from the probability distributions for each UN region.

### 3.3. Global Emissions Inventories Comparison

Figure 22 below shows the comparison between the EDGAR v7.0 dataset and our release of emissions estimates for all 10,000 GHSL-defined urban centers in our dataset. While there is a strong correlation across all emissions, there are also significant differences for some urban centers. For example, where EDGAR broadly predicts  $10^2$  to  $10^4$  tons, our methodology predicts more. Where EDGAR broadly predicts  $10^4$  to  $10^6$  tons, our methodology predicts less. Our methodology produces lower emissions estimates roughly 62% of the time. This might be an artifact of the comparison method or the underlying estimation framework. For the purposes of this methodology document, we simply highlight that the two datasets provide comparable estimates when taken in aggregate.

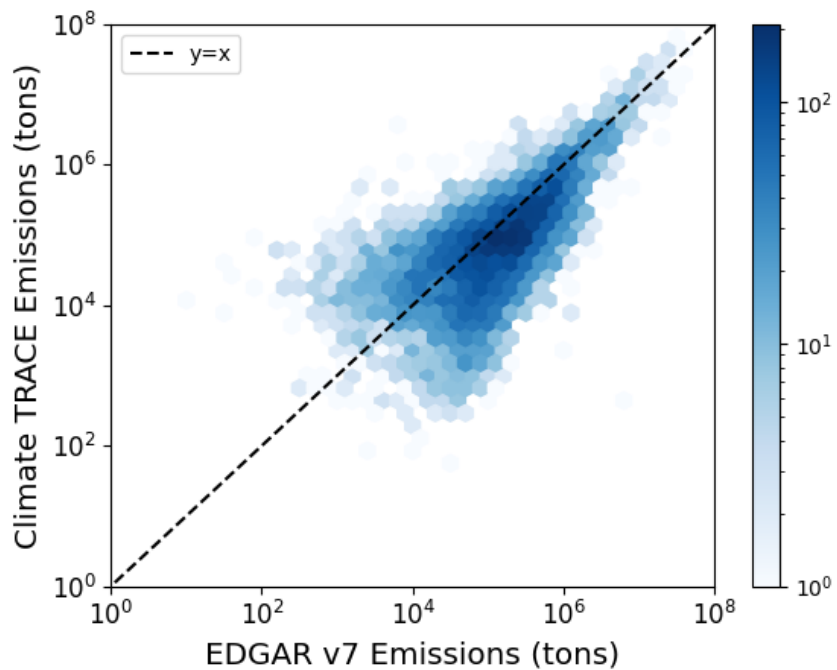


**Figure 21** Comparison of EDGAR v7 emissions and estimates described in this methodology across 10,000 urban centers expressed as a two-dimensional histogram binned on hexagons. Darker blues indicate that the most common comparison between the two databases indicates that our methodology under-estimates emissions relative to EDGAR.

Our emissions estimates are broadly comparable to EDGAR v7 data as shown in Figure 22. Potential sources of discrepancies between the emissions inventories warrant further investigation, including timespan differences and varying geographic extents for each city. A key strength of our approach is the ease with which our estimates can be updated as better data become available, as well as the ability to run our pipeline over more cities and/or larger regions.

Further international validation for both AADT and resulting emissions estimates is necessary, including a deeper understanding of all potential sources of differences (e.g., emissions factors uncertainty, varying total road network length included, etc.). We aim to incorporate more

international AADT datasets, where available, into our model training and validation process. The addition of more real-time data (e.g., traffic and mobility) will help address the temporal ambiguity of our estimates. Finding publicly available data of this type remains a significant challenge.

### 3.4. Worldwide Emissions Results

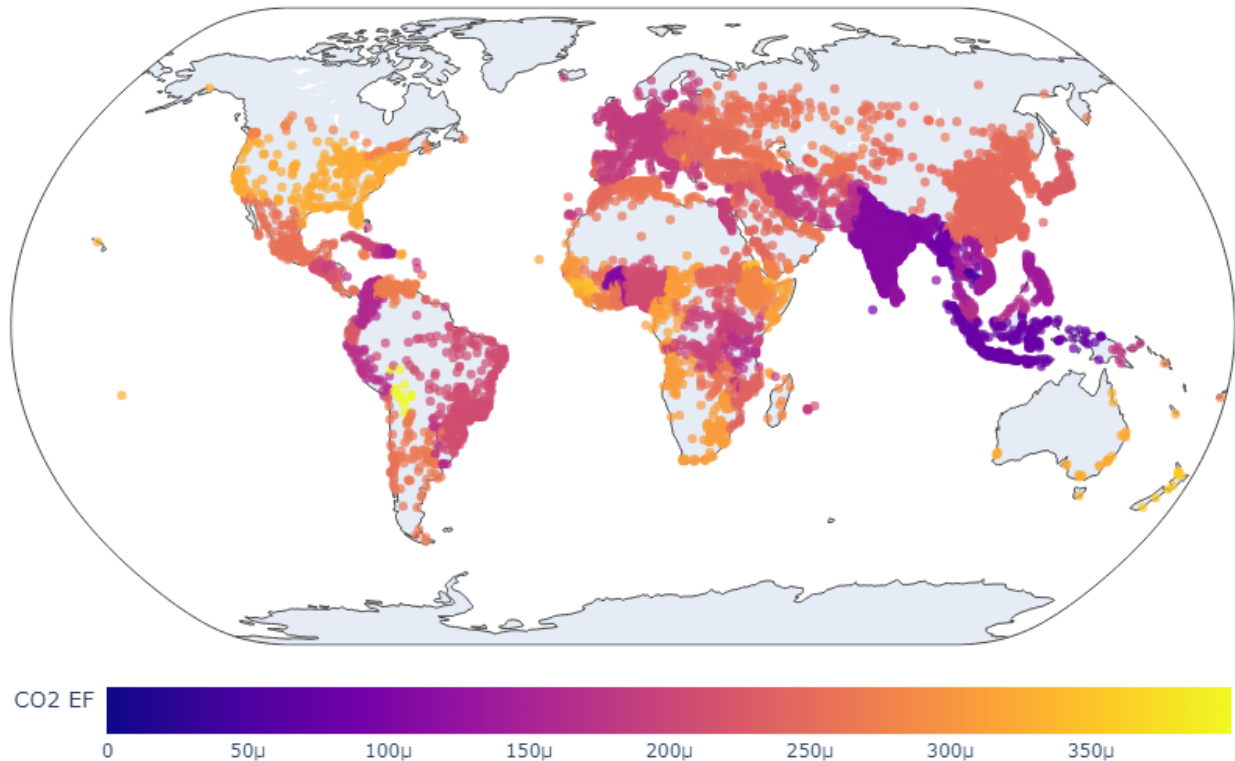


**Figure 22** Global map of the 2022 emissions factor for all urban areas in the released data set. Units are tonnes per VKT (100 μTonnes/VKT ↔ 100 g/VKT).

Figure 22 above shows an overview of the emissions factors (EF, see section 2.2.10). One interesting highlight from our data is the fact that urban areas in India and Indonesia have a much lower EF than countries such as China or even the US. This is mostly due to our data sources for vehicle fleet mix in those countries, which indicate that a vast majority of vehicles in those two countries are motorcycles. This is highlighted in Figure 23 below: Indonesia and India have vehicle registrations around 75% for motorcycles.

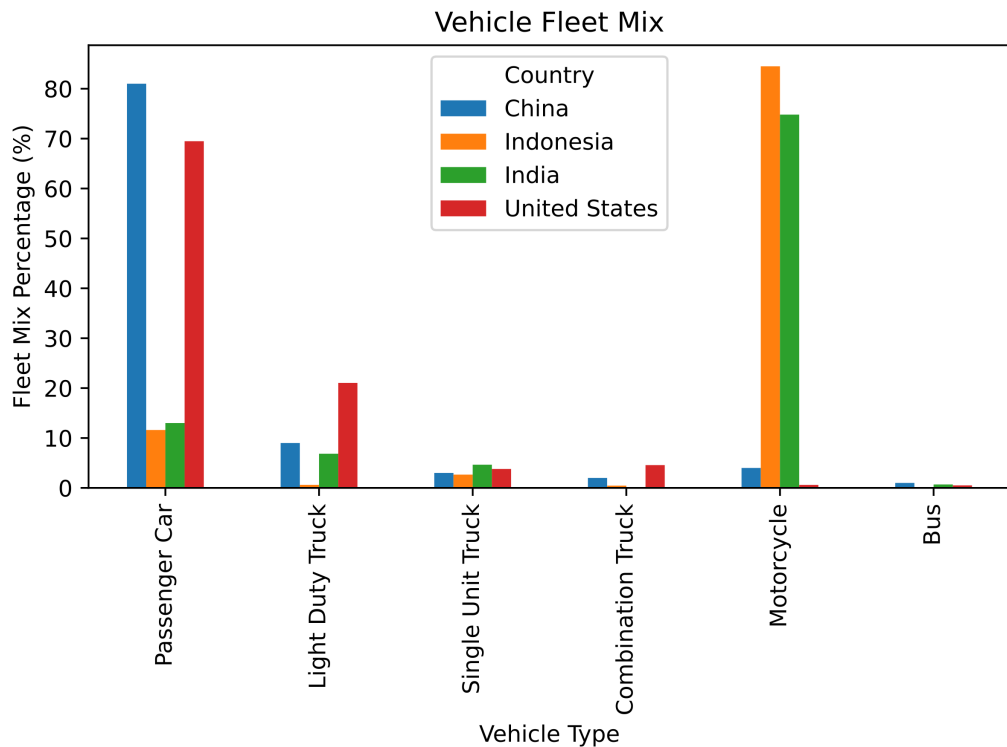


**Figure 23** Vehicle fleet mix for four countries highlighting the difference in motorcycle usage.

Additional highlights include:

- We estimate that between 2021 and 2022, an extra  $71 \times 10^6$  extra tonnes of CO<sub>2</sub> were emitted from road transportation; this is a 2.3% increase
- Of this 2.3% increase, 25% of the increase is attributable to HIC, 43% to UMIC, 29% to LMIC, and 3% to LIC<sup>2</sup>
- Of the 2022 estimated emissions, 49% is from HIC, 31% UMIC, 16% LMIC, 3% LIC

#### 4. Conclusions

We have presented a hybrid road transportation emissions estimation method that is detailed, scalable, and easy to update. The ability to calculate emissions per road segment can be further refined to reach an unprecedented level of detail and global coverage. Where available, the integration of real-time traffic data would increase the temporal resolution and accuracy of our models. This type of actionable emissions monitoring data will be critical to ensuring we meet global emissions reduction targets and may inspire new ways of mitigating the effects of climate change. Finally, more local vehicle registration or usage data would improve our emissions estimates regardless of a change in the underlying model predictions of average traffic.

<sup>2</sup> HIC: High income country, UMIC: Upper-middle income country, LMIC: Lower-middle income country, LIC: Low-income country, as defined by the World Bank: <https://datahelpdesk.worldbank.org/knowledgebase/articles/906519>.

Our uncertainty estimates are large (see section 3.2) partly due to very conservative assumptions about error sources. We believe a fuller Monte-Carlo simulation of different error sources from the source data (such as fuel mix, vehicle mix, etc.) will provide a more accurate error analysis in the future. Additionally, we will attempt better estimates of per-road-segment activity estimates by comparing against AADT (or equivalent) ground truth values in countries other than the US. Finally, we will need to estimate road network effects in more detail on a per-country or region level.

## 5. Acknowledgements

Thanks to Gabriela Volpato, Aaron Davitt, and Lekha Sridhar from WattTime for their help in reviewing our methodology. We thank two APL ASPIRE Interns, Melat Ghebreselassie and Kevin Zhang, for their work in extending the vehicle fleet database to many additional countries.

## 6. Supplementary Materials

### 1.1. Vehicle Fleet Mix Sources

The following standard references are used:

- The following countries use the ACEA dataset: (ACEA - European Automobile Manufacturers' Association 2022).
  - Russian Federation
  - Republic of Turkiye
  - United Kingdom of Great Britain and Northern Ireland
  - Federal Republic of Germany
  - French Republic
  - Kingdom of Spain
  - Italian Republic
  - Republic of Poland
  - Kingdom of the Netherlands
  - Portuguese Republic
  - Kingdom of Belgium
  - Kingdom of Sweden
  - Czech Republic
  - Kingdom of Denmark
  - Ireland
  - Republic of Finland
- The following countries use the UNECE dataset: (UNECE - United Nations Economic Commission for Europe 2022)
  - Hellenic Republic
  - Republic of Belarus
  - State of Israel

- Republic of Azerbaijan
  - Swiss Confederation
  - Republic of Hungary
  - Republic of Austria
  - Republic of Bulgaria
  - Republic of Croatia
  - Republic of Albania
  - Republic of Lithuania
  - Republic of Moldova
  - Bosnia and Herzegovina
  - Republic of Latvia
  - Republic of Cyprus
  - Republic of Estonia
  - Republic of Slovenia
  - Republic of Malta
  - Republic of Iceland
  - Grand Duchy of Luxembourg
  - Montenegro
- The following countries use the WHO (World Health Organization 2018)
  - Republic of Indonesia
  - Japan
  - Arab Republic of Egypt
  - Islamic Republic of Iran
  - Republic of the Philippines
  - Republic of Colombia
  - Republic of Iraq
  - Kingdom of Thailand
  - Bolivarian Republic of Venezuela
  - Republic of the Sudan
  - Kingdom of Morocco
  - Republic of Peru
  - Republic of Ghana
  - Commonwealth of Australia
  - United Republic of Tanzania
  - Islamic Republic of Afghanistan
  - Republic of Ecuador
  - Republic of Cote d'Ivoire
  - Republic of Senegal

- Syrian Arab Republic
- Republic of Kazakhstan
- United Arab Emirates
- Democratic Socialist Republic of Sri Lanka
- Dominican Republic
- Romania
- Plurinational State of Bolivia
- Federal Democratic Republic of Nepal
- Republic of Tunisia
- Burkina Faso
- Republic of Cuba
- Republic of Guinea
- Republic of Zimbabwe
- Republic of Benin
- State of Palestine
- Lebanese Republic
- Togolese Republic
- Republic of Paraguay
- State of Libya
- Republic of Honduras
- Republic of El Salvador
- Kingdom of Cambodia
- Republic of Madagascar
- Republic of Costa Rica
- Republic of Burundi
- Republic of Panama
- Oriental Republic of Uruguay
- Republic of South Sudan
- State of Eritrea
- Republic of Liberia
- Sultanate of Oman
- Republic of Rwanda
- Mongolia
- Kingdom of Norway
- Republic of the Gambia
- Slovak Republic
- Republic of Botswana

- Lao People's Democratic Republic
  - Republic of Trinidad and Tobago
  - Republic of Mauritius
  - Republic of Namibia
  - Democratic Republic of Timor-Leste
  - Co-operative Republic of Guyana
  - Republic of Suriname
  - Republic of Maldives
  - Barbados
  - Belize
- Other Countries for which we have specific data:
  - Argentina (ARG): (ADEFA n.d.)
  - Australia (AUS): (“Motor Vehicle Census, Australia, 31 Jan 2021 | Australian Bureau of Statistics” 2021)
  - Brazil (BRA): (“Fleet Size of the Auto Industry in Brazil by Type 2021” 2022)
  - Canada (CAN); (Government of Canada 2020)
  - Chile (CHL) <https://www.ine.cl/docs/default-source/parque-...>
  - People’s Republic of China (CHN)
  - Guatemala (GTM)
  - India (IND): Road Transport Yearbook
  - Indonesia (IDN)
  - Japan (JPN)
  - Kuwait (KWT)
  - Malaysia (MYS)
  - Myanmar (MMR)
  - Singapore (SGP)

## 1.2. Supplementary materials metadata

**Table S1** General dataset information

General Description	Definition
<b>Sector definition</b>	Emissions from all road-based transportation such as cars, buses, motorcycles, and trucks.
<b>UNFCCC sector equivalent</b>	1.A.3.b (“Road Transportation”)
<b>Temporal Coverage</b>	2021 – 2022
<b>Temporal Resolution</b>	Annual
<b>Data format(s)</b>	Compressed CSV
<b>Coordinate Reference System</b>	EPSG:4326, decimal degrees
<b>Number of sources available for download and percent of global emissions (as of 2022)</b>	Almost 18,000 urban areas total covering approximately 45% of the world’s population
<b>Total emissions for 2022</b>	$3.14 \times 10^9$ tonnes of CO <sub>2</sub> e
<b>Ownership</b>	N/A: estimates rely on modeling individual vehicles; no ownership is possible.
<b>What emission factors were used?</b>	Model based
<b>What is the difference between a “NULL / none” versus “0” data field?</b>	“0” values are for true non-existent emissions. If we know that the sector has emissions for that specific gas, but the gas was not modeled, this is represented by “NULL/none/nan”
<b>total_CO2e_100yrGWP total_CO2e_20yrGWP conversions</b>	and Climate TRACE uses IPCC AR6 CO <sub>2</sub> e GWPs. CO <sub>2</sub> e conversion guidelines are here:

[https://www.ipcc.ch/report/ar6/wg1/downloads/report/IPCC\\_AR6\\_WGI\\_FullReport\\_small.pdf](https://www.ipcc.ch/report/ar6/wg1/downloads/report/IPCC_AR6_WGI_FullReport_small.pdf)

**Table S2** Source level metadata description

Data attribute	Definition
<b>sector</b>	Transportation
<b>source_sub-sector_name</b>	Road transportation
<b>source_definition</b>	Emissions from on-road transportation within an urban area defined by GHSL-UCSD extent divided into GADM based administrative areas. See Section 2.2.2.
<b>start_date</b>	Start date for time period of emissions estimation (YYYY-MM-DD format)
<b>end_date</b>	End date for time period of emissions estimation (YYYY-MM-DD format)
<b>source_identifier</b>	Internal, unique ID for urban area (float). The GHSL-UCDB urban center can be recovered by grouping on the floor of the source_identifier.
<b>source_name</b>	Urban area subdivision
<b>iso3_country</b>	ISO 3166-1 alpha-3 country code for city taken from GADM ADM_2 layer value
<b>location</b>	Well-known text (WKT) MultiPolygon of city geographic bounds, in WGS 84 - EPSG:4326 coordinate reference system (CRS).
<b>type</b>	Not used; N/A

Data attribute	Definition
<b>capacity_description</b>	Total road network length for each urban area
<b>capacity_units</b>	kilometers
<b>capacity_factor_description</b>	Not used; N/A
<b>capacity_factor_units</b>	Not used; N/A
<b>activity_description</b>	Total vehicle kilometers traveled (VKT) per urban area. See Section 2.2.10
<b>activity_units</b>	vehicle-kilometers
<b>CO2_emissions_factor</b>	tonnes CO <sub>2</sub> /VKT; see Section 2.2.10
<b>CH4_emissions_factor</b>	tonnes CH <sub>4</sub> /VKT; see Section 2.2.10
<b>N2O_emissions_factor</b>	tonnes N <sub>2</sub> O/VKT; see Section 2.2.10
<b>other_gas_emissions_factor</b>	Not used; N/A
<b>CO2_emissions</b>	tonnes CO <sub>2</sub> ; see Section 2.2.10
<b>CH4_emissions</b>	tonnes CH <sub>4</sub> ; see Section 2.2.10
<b>N2O_emissions</b>	tonnes N <sub>2</sub> O; see Section 2.2.10
<b>other_gas_emissions</b>	Not used; N/A
<b>total_CO2e_100yrGWP</b>	tonnes CO <sub>2</sub> e; see Section 2.2.10

Data attribute	Definition
<b>total_CO2e_20yrGWP</b>	tonnes CO <sub>2</sub> e; see Section 2.2.10
<b>other1_description</b>	The GHSL provided ISO 3166-1 alpha-3 country code (it might differ from the GADM assigned alpha-3 country code)
<b>other1_units</b>	N/A
<b>other2_description</b>	The GHSL urban center name of the overarching
<b>other2_units</b>	N/A
<b>other3_description</b>	N/A
<b>other3_units</b>	N/A
<b>other4_description</b>	N/A
<b>other4_units</b>	N/A
<b>other5_description</b>	N/A
<b>other5_units</b>	N/A
<b>other6_description</b>	N/A
<b>other6_units</b>	N/A
<b>other7_description</b>	N/A
<b>other7_units</b>	N/A

Data attribute	Definition
<b>other8_description</b>	N/A
<b>other8_units</b>	N/A
<b>other9_description</b>	N/A
<b>other9_units</b>	N/A
<b>other10_description</b>	N/A
<b>other10_units</b>	N/A

**Table S3** Source level metadata description confidence and uncertainty

Data attribute	Confidence Definition	Uncertainty Definition
<b>type</b>		
<b>capacity_description</b>	See Section 3.2.7	See Section 3.2.2
<b>capacity_units</b>	See Section 3.2.7	Kilometers
<b>capacity_factor_description</b>	See Section 3.2.7	N/A
<b>capacity_factor_units</b>	See Section 3.2.7	N/A
<b>activity_description</b>	See Section 3.2.7	See Section 3.2.3
<b>activity_units</b>	See Section 3.2.7	vehicle-kilometers
<b>CO2_emissions_factor</b>	See Section 3.2.7	See Section 3.2.5

Data attribute	Confidence Definition	Uncertainty Definition
<b>CH4_emissions_factor</b>	See Section 3.2.7	See Section 3.2.5
<b>N2O_emissions_factor</b>	See Section 3.2.7	See Section 3.2.5
<b>other_gas_emissions_factor</b>	See Section 3.2.7	N/A
<b>CO2_emissions</b>	See Section 3.2.7	See Section 3.2.4
<b>CH4_emissions</b>	See Section 3.2.7	See Section 3.2.4
<b>N2O_emissions</b>	See Section 3.2.7	See Section 3.2.4
<b>other_gas_emissions</b>	See Section 3.2.7	N/A
<b>total_CO2e_100yrGWP</b>	See Section 3.2.7	See Section 3.2.6
<b>total_CO2e_20yrGWP</b>	See Section 3.2.7	See Section 3.2.6

## 2. Administrative Concerns

### 2.1. Permissions and Use

All Climate TRACE data is freely available under the Creative Commons Attribution 4.0 International Public License, unless otherwise noted below.

### 2.2. Citation format

Tomek M. Kott, Kevin Foster, Elizabeth Reilly, and Marisa Hughes (2023). *Transportation Sector: Urban Area-level Road Transportation Emissions*. The Johns Hopkins University Applied Physics Laboratory (JHU/APL), Laurel, MD, USA, Climate TRACE Emissions Inventory. <https://climatetrace.org> [Accessed date]

### 2.3. Geographic boundaries and names (iso3\_country data attribute):

The depiction and use of boundaries, geographic names and related data shown on maps and included in lists, tables, documents, and databases on Climate TRACE are generated from the Global Administrative Areas (GADM) project (Version 4.1 released on 16 July 2022) along with their corresponding ISO3 codes, and with the following adaptations:

- HKG (China, Hong Kong Special Administrative Region) and MAC (China, Macao Special Administrative Region) are reported at GADM level 0 (country/national);
- Kosovo has been assigned the ISO3 code ‘XKX’;
- XCA (Caspian Sea) has been removed from GADM level 0 and the area assigned to countries based on the extent of their territorial waters;
- XAD (Akrotiri and Dhekelia), XCL (Clipperton Island), XPI (Paracel Islands) and XSP (Spratly Islands) are not included in the Climate TRACE dataset;
- ZNC name changed to ‘Turkish Republic of Northern Cyprus’ at GADM level 0;
- The borders between India, Pakistan and China have been assigned to these countries based on GADM codes Z01 to Z09.

The above usage is not warranted to be error free and does not imply the expression of any opinion whatsoever on the part of Climate TRACE Coalition and its partners concerning the legal status of any country, area or territory or of its authorities, or concerning the delimitation of its borders.

#### **2.4. Disclaimer**

The emissions provided for this sector are our current best estimates of emissions, and we are committed to continually increasing the accuracy of the models on all levels. Please review our terms of use and the sector-specific methodology documentation before using the data. If you identify an error or would like to participate in our data validation process, please [contact us](#).

### **3. References**

4. ACEA - European Automobile Manufacturers' Association. 2022. “Report - Vehicles in Use, Europe 2022.” <https://www.acea.auto/publication/report-vehicles-in-use-europe-2022/>.
5. ADEFA. n.d. “Anuario 2020 | Estadísticas.” ADEFA. Accessed December 14, 2022. <http://adefa.org.ar/es/estadisticas-anuarios-interno?id=55>.
6. Boeing, Geoff. 2017. “OSMnx: New Methods for Acquiring, Constructing, Analyzing, and Visualizing Complex Street Networks.” *Computers, Environment and Urban Systems* 65 (September): 126–39. <https://doi.org/10.1016/j.compenvurbsys.2017.05.004>.
7. Bronstein, Michael M., Joan Bruna, Yann LeCun, Arthur Szlam, and Pierre Vandergheynst. 2017. “Geometric Deep Learning: Going beyond Euclidean Data.” *IEEE Signal Processing Magazine* 34 (4): 18–42. <https://doi.org/10.1109/MSP.2017.2693418>.
8. Crippa, Monica, Efisio Solazzo, Ganlin Huang, Diego Guizzardi, Ernest Koffi, Marilena Muntean, Christian Schieberle, Rainer Friedrich, and Greet Janssens-Maenhout. 2020. “High Resolution Temporal Profiles in the Emissions Database for Global Atmospheric Research.” *Scientific Data* 7 (1): 1–17. <https://doi.org/10.1038/s41597-020-0462-2>.
9. Drusch, Matthias, Umberto Del Bello, Sébastien Carlier, Olivier Colin, Veronica Fernandez, Ferran Gascon, Bianca Hoersch, et al. 2012. “Sentinel-2: ESA’s Optical High-Resolution Mission for GMES Operational Services.” *Remote Sensing of Environment*.
10. Fan, Tongle, Guanglei Wang, Yan Li, and Hongrui Wang. 2020. “MA-Net: A Multi-Scale Attention Network for Liver and Tumor Segmentation.” *IEEE Access*.

11. “Fleet Size of the Auto Industry in Brazil by Type 2021.” 2022. *Statista*. <https://www.statista.com/statistics/787327/automobile-industry-fleet-size-brazil-vehicle-type/>.
12. Florczyk, A., C. Corbane, M. Schiavina, M. Pesaresi, L. Maffenini, M. Melchiorri, P. Politis, et al. 2019. “GHS Urban Centre Database 2015, Multitemporal and Multidimensional Attributes, R2019A.” European Commission, Joint Research Centre (JRC). <https://data.jrc.ec.europa.eu/dataset/53473144-b88c-44bc-b4a3-4583ed1f547e>.
13. Forster, P., Storelvmo, T., Armour, K., Collins, W., and Dufresne, J.-L., Frame, D., Lunt, D.J., Mauritzen, T., Palmer, M.D., Watanabe, M., Wild, M., and Zhang, H. 2023. “The Earth’s Energy Budget, Climate Feedbacks and Climate Sensitivity.” In *Climate Change 2021 – The Physical Science Basis: Working Group I Contribution to the Sixth Assessment Report of the Intergovernmental Panel on Climate Change*, 923–1054. Cambridge: Cambridge University Press. <https://doi.org/10.1017/9781009157896.009>.
14. Gately, Conor K, L.R. Hutyra, and I.S. Wing. 2019. “DARTE Annual On-Road CO<sub>2</sub> Emissions on a 1-Km Grid, Conterminous USA V2, 1980-2017.” ORNL Distributed Active Archive Center. <https://doi.org/10.3334/ORNLDAAAC/1735>.
15. Gately, Conor K, Lucy R Hutyra, and Ian Sue Wing. 2015. “Cities, Traffic, and CO<sub>2</sub>: A Multidecadal Assessment of Trends, Drivers, and Scaling Relationships.” *Proceedings of the National Academy of Sciences*.
16. Global Administrative Areas. 2022. “GADM Database of Global Administrative Areas, Version 4.1.” <https://www.gadm.org>.
17. Government of Canada, Statistics Canada. 2020. “Vehicle Registrations, by Type of Vehicle, Inactive.” September 10, 2020. <https://www150.statcan.gc.ca/t1/tbl1/en/tv.action?pid=2310006701>.
18. Gurney, Kevin R, Jianming Liang, Risa Patarasuk, Yang Song, Jianhua Huang, and Geoffrey Roest. 2020. “The Vulcan Version 3.0 High-Resolution Fossil Fuel CO<sub>2</sub> Emissions for the United States.” *Journal of Geophysical Research: Atmospheres*.
19. International Energy Agency. 2019. “Transport Sector CO<sub>2</sub> Emissions by Mode in the Sustainable Development Scenario, 2000-2030 – Charts – Data & Statistics.” IEA. March 27, 2019. <https://www.iea.org/data-and-statistics/charts/transport-sector-co2-emissions-by-mode-in-the-sustainable-development-scenario-2000-2030>.
20. Jochen Topf. 2023. “Osmium: Command Line Tool for Working with OpenStreetMap Data Based on the Osmium Library.” <https://osmcode.org/osmium-tool/>.
21. Liu, Zhu, Philippe Ciais, Zhu Deng, Steven Davis, Bo Zheng, Yilong Wang, Duo Cui, et al. 2020. “Carbon Monitor, a near-Real-Time Daily Dataset of Global CO<sub>2</sub> Emission from Fossil Fuel and Cement Production.” *Scientific Data* 7 (November). <https://doi.org/10.1038/s41597-020-00708-7>.
22. Main-Knorn, M., B. Pflug, J. Louis, V. Debaecker, U. Müller-Wilm, and F. Gascon. 2017. “Sen2Cor for Sentinel-2.” In *Image and Signal Processing for Remote Sensing XXIII*, 10427:37–48. IEEE.
23. Microsoft Bing Maps. 2023. “Road Detections.” Microsoft. <https://github.com/microsoft/RoadDetections>.
24. “Motor Vehicle Census, Australia, 31 Jan 2021 | Australian Bureau of Statistics.” 2021. June 30, 2021.

- <https://www.abs.gov.au/statistics/industry/tourism-and-transport/motor-vehicle-census-australia/latest-release>.
25. Mukherjee, Ryan, Derek Rollend, Gordon Christie, Armin Hadzic, Sally Matson, Anshu Saksena, and Marisa Hughes. 2021. “Towards Indirect Top-Down Road Transport Emissions Estimation.” In *2021 IEEE/CVF Conference on Computer Vision and Pattern Recognition Workshops (CVPRW)*, 1092–1101. <https://doi.org/10.1109/CVPRW53098.2021.00120>.
  26. OpenStreetMap Contributors. 2020. “OpenStreetMap: User-Generated Street Maps.” <https://planet.osm.org>.
  27. Scheibenreif, Linus M., Michael Mommert, and Damian Borth. 2021. “Estimation of Air Pollution with Remote Sensing Data: Revealing Greenhouse Gas Emissions from Space.” In *ICML 2021 Workshop on Tackling Climate Change with Machine Learning*. <https://www.climatechange.ai/papers/icml2021/23>.
  28. UNECE - United Nations Economic Commission for Europe. 2022. “Road Vehicle Fleet at 31 December by Fuel Type, Type of Vehicle, Country and Year.” [https://w3.unece.org/PXWeb2015PXWeb2015/pxweb/en/STAT/STAT\\_40-TRTRANS\\_03-TRRoadFleet/03\\_en\\_TRRoadFuelFlt\\_r.px/](https://w3.unece.org/PXWeb2015PXWeb2015/pxweb/en/STAT/STAT_40-TRTRANS_03-TRRoadFleet/03_en_TRRoadFuelFlt_r.px/).
  29. US EPA. 2022. “GHG Emissions Factors Hub.” [https://www.epa.gov/system/files/documents/2022-04/ghg\\_emission\\_factors\\_hub.pdf](https://www.epa.gov/system/files/documents/2022-04/ghg_emission_factors_hub.pdf).
  30. ———. 2023. “Inventory of U.S. Greenhouse Gas Emissions and Sinks: 1990–2021.” <https://www.epa.gov/ghgemissions/inventory-us-greenhouse-gas-emissions-and-sinks-1990-2021>.
  31. US FHWA. 2017. “Highway Performance Monitoring System (HPMS) Data.” <https://www.fhwa.dot.gov/policyinformation/hpms>.
  32. ———. 2018. “State Motor-Vehicle Registrations.” <https://www.fhwa.dot.gov/policyinformation/statistics/2018/mv1.cfm>.
  33. ———. 2020. “Distribution of Annual Vehicle Distance Traveled - Percentage by Vehicle Type Rural/Urban (Table VM-4).” <https://www.fhwa.dot.gov/policyinformation/statistics/2020/vm4.cfm>.
  34. Veličković, Petar, Guillem Cucurull, Arantxa Casanova, Adriana Romero, Pietro Liò, and Yoshua Bengio. 2018. “Graph Attention Networks.” In . <https://openreview.net/forum?id=rJXMpikCZ>.
  35. World Bank Group. 2019. “CURB: Climate Action for Urban Sustainability, Version 2.1.” <https://datacatalog.worldbank.org/search/dataset/0042029>.
  36. World Health Organization. 2018. *Global Status Report on Road Safety 2018*. Genève, Switzerland: World Health Organization. <https://www.who.int/publications-detail-redirect/9789241565684>.
  37. World Resources Institute. 2022. “Greenhouse Gas (GHG) Emissions | Climate Watch.” 2022. <https://www.climatewatchdata.org/ghg-emissions>.